ANL-7017

ANL-7017

Argonne National Laboratory

REACTOR DEVELOPMENT PROGRAM

PROGRESS REPORT

February 1965

LEGAL NOTICE

Printed in USA. Price $3.00. Available from the Clearinghouse for Federal Scientific and Technical Information, National Bureau of Standards, U. S. Department of Commerce, Springfield, Virginia

DISCLAIMER

ANL-7017
Reactor Technology
(TID-4500, 37th Ed.)
AEC Research and
Development Report

ARGONNE NATIONAL LABORATORY
9700 South Cass Avenue
Argonne, Illinois 60440

REACTOR DEVELOPMENT PROGRAM PROGRESS REPORT

February 1965

Albert V Crewe, Laboratory Director
Stephen Lawroski, Associate Laboratory Director

Division	Director
Chemical Engineering	R. C Vogel
Idaho	M. Novick
Metallurgy	F. G Foote
Reactor Engineering	L. J. Koch
Reactor Physics	R. Avery
Remote Control	R. C Goertz

Report Coordinated by
R. M. Adams and A. Glassner

Issued March 18, 1965

Operated by The University of Chicago
under
Contract W-31-109-eng-38
with the
U. S. Atomic Energy Commission

FOREWORD

The Reactor Development Program Progress Report, issued monthly, is intended to be a means of reporting those items of significant technical progress which have occurred in both the specific reactor projects and the general engineering research and development programs. The report is organized in a way which, it is hoped, gives the clearest, most logical over-all view of progress. The budget classification is followed only in broad outline, and no attempt is made to report separately on each sub-activity number. Further, since the intent is to report only items of significant progress, not all activities are reported each month. In order to issue this report as soon as possible after the end of the month editorial work must necessarily be limited. Also, since this is an informal progress report, the results and data presented should be understood to be preliminary and subject to change unless otherwise stated.

The issuance of these reports is not intended to constitute publication in any sense of the word. Final results either will be submitted for publication in regular professional journals or will be published in the form of ANL topical reports.

The last six reports issued in this series are:

August 1964	ANL-6936
September 1964	ANL-6944
October 1964	ANL-6965
November 1964	ANL-6977
December 1964	ANL-6997
January 1965	ANL-7003

Reactor Development Program
Highlights of Project Activities for
February, 1965

EBR-II

During the month of February, EBR-II was reloaded with additional fuel in preparation for resumption of power operation. Also, six subassemblies that had been in the reactor for a maximum of about 0.25 a/o burnup, were removed for disassembly and inspection in the Fuel Cycle Facility.

A pinhole leak (from water to air) was discovered in evaporator 702 and repairs were begun. It is expected that repair can be completed in early March.

FARET

An updated cost estimate prepared in February indicated only a slight increase, but still within the authorized limit.

The A-E Title II design of the plant is about 90% complete.

The cell design has been modified somewhat to incorporate a system which will make it possible to have ready manual access to the control rod drives and reactor vessel cover.

ZPPR

The Title I report on the ZPPR facility was issued on February 16, 1965, by the Architect-Engineer, Mason and Hanger, Silas Mason Co., Inc. Title II work was also started in February.

The bid package for the reactor bed and tables was sent to prospective bidders.

AARR

Authorization was received during February from the AEC to negotiate a contract with the architect engineering firm of Burns and Roe, Inc., New York.

Plutonium Recycle Program (EBWR)

Nondestructive examination of the primary equipment, piping, auxiliary equipment and vessel cladding of EBWR has been completed. This examination has indicated defects of various kinds in a large number of welds, none of which were radiographed originally. These welds will be replaced, along with some piping. The work will probably not be completed in less than about 3 months. Some cracking of the vessel cladding has been observed, but it is not considered to be a safety problem.

TABLE OF CONTENTS

TABLE OF CONTENTS

TABLE OF CONTENTS

I. LIQUID-METAL-COOLED REACTORS

A. EBR-II

1. Operations

Fuel was reloaded into the reactor in preparation for the resumption of operation. Six subassemblies (one inner blanket, one special core-type surveillance, one control rod, two 6th-row core, and one outer blanket) that had been in the reactor for a maximum of approximately 0.25 a/o burnup were transferred from reactor grid positions to the storage basket, and then to the Fuel Cycle Facility for disassembly and examination (see Section I. A. 6. d. below). Also, the six dummy subassemblies which had been installed to permit removal of control rod thimble No. 8 were replaced with standard, core-type and inner blanket subassemblies.

The temperature of the bulk sodium in the primary tank was increased gradually for three days to 700°F. This was done to permit replacement of a number of subassembly outlet thermocouples located in the reactor vessel cover.

With the primary system in operation, the cold trap was used to reduce the plugging temperature from 320 to 250°F. The cold trap was then secured, but flow was maintained through the bypass. During the first half of the month, the hydrogen content of the primary cover gas increased from 1900 ppm to about 16,000 ppm. This increase was attributed to the inevitable admission of moisture and air to the primary tank during the removal of the oscillator rod and thimble, and during other work involving movement of tools and components through the primary tank cover. The hydrogen content has been slowly reduced during the latter part of the month.

The secondary recirculation system was placed in operation with bypass of the cold trap to run some special electrical tests with the electromagnetic pumps. During this period, the plugging temperature of the sodium in the storage tank was 280°F. Following the tests, the system was allowed to freeze. Data are being analyzed, but it is apparent that the pumps have quite different electrical characteristics. The composition of the secondary cover gas remained stable, containing about 10 ppm of hydrogen and about 6000 ppm of nitrogen. The system was purged and filled with fresh argon to reduce the nitrogen content.

During a site-wide power failure, the 400-kW diesel generator started, loaded normally, and then stopped. This failure of the diesel was accompanied by a loss of annunciation in the control room, for the constant-process-power MG set was not carrying the process instrument load at the time of failure. This combination of circumstances prevented accurate determination of the cause of the diesel failure. However, subsequent investigation

showed that the diesel stopped because of lack of lubrication oil pressure. Two steps have been taken to reduce the possibility of recurrence. First, the oil temperature in the crankcase is being maintained at 100°F or higher; second, the time-delay relay which bypasses the oil-pressure switch during startup has been set for longer delay time.

Investigation also revealed that the diesel cannot be restarted after a failure of this kind until the diesel-control switch in the control room has been placed in "off" momentarily and back to "standby." Lack of this information prevented manual restarting of the diesel during the power outage. This information will be incorporated in the operating instructions.

Frequent tests of the emergency power system are being conducted to verify the reliability of the diesel generators. A possible change in the location of the diesel-control switch from the control room to the auxiliary boiler room (near the diesel engine) is being studied.

2. Examination of Failed Oscillator Rod and Thimble

The oscillator rod and thimble and control rod thimble No. 8 were examined in a shielded cell. After disassembly, no debris was found except small ball bearings from the lower guide bushing of the oscillator drive. The oscillator guide thimble and the control rod guide thimble had seized because three balls jammed above the upper piston of the oscillator rod guide thimble. The scoring marks were comparatively light. Four balls were found above the lower piston, but this section had not seized. One ball was found in the spring plunger cavity.

The oscillator rod was jammed by 19 balls in the lower portion of the guide sleeve. Very heavy scoring was observed in two of the three lower guides on the oscillator rod and in the corresponding guide slots of the guide tube. Some fairly heavy scoring marks were also observed on the oscillator rod and lower guide tube above the lower oscillator rod guide. A total of 27 balls were found during disassembly.

The disassembly procedure and findings were as follows: One slitting cut in the lower adapter of the control rod was made on a milling machine. All other cuts were made with a portable abrasive cutting saw. All parts were subjected to close visual inspection and photographed with the variable power hot-cell periscope.

(i) A circumferential cut was made in the hexagonal tube of the control rod thimble $39\frac{3}{4}$ in. from the bottom. The hex can of the control rod thimble was free and was separated from the oscillator guide thimble. The lower adapter of the control rod thimble remained in the oscillator rod guide thimble.

(ii) A circumferential cut was made at the inlet part of the lower adapter of the control rod thimble. The bottom end of the control rod thimble was free and was pulled off the oscillator guide thimble bottom end. Four balls fell out. One was deformed.

(iii) The oscillator guide tube was cut transversely just above the 1/2-in. key bar at the bottom of the guide tube section. Each piece was suspended, but no balls came out.

(iv) The lower part of the oscillator rod guide thimble and the control rod thimble lower adapter still seized to it were placed in the mill. The control rod thimble lower adapter was slit longitudinally and pulled free of the oscillator rod upper piston. Three balls were found. Score marks on the piston were light.

(v) The lower piston was cut off the oscillator guide thimble. The spring and plunger came out. One ball was found in this cavity.

(vi) The oscillator rod guide tube was cut transversely 17 in. from the top. The top section of the tube pulled free. No balls came out.

(vii) The oscillator thimble was cut transversely 36 in. from the top of the oscillator rod, just below the bottom of the oscillator rod.

(viii) The remaining guide tube section was slit longitudinally on one side; it did not come free. It was then slit on the opposite side opening it into two halves. The oscillator rod has deep gouges in two of the three lower guides. Some short, parallel score marks were found on the rod above the guides. The corresponding guide slots in the tube also showed heavy score marks with extruded metal at one end (possibly an imbedded ball). There were short longitudinal score marks in the wear sleeve above the heaviest gouges. Nineteen balls were found in this region. One was heavily deformed.

3. Check of Control and Safety Rods

The safety rods were checked for possible binding by counterweighting the weight of the drive and slowly lifting the rods to the fuel-handling elevation. Each rod was then removed by means of gripper. A special tool was lowered into each thimble to determine if any debris could be found on the shoulder area located at the top of the guide-tube position of the safety rod thimble. The tool contained a flat aluminum disc and a plunger arrangement which was designed to dislodge any debris present on the shoulder. The aluminum disc was then brought in contact with the shoulder; it was assumed that any debris present on the shoulder would mark the contacting aluminum surface. No evidence of debris was found. After the safety rods were reinstalled, the drive was manually lowered and raised twice. No binding of the rods in the thimbles was observed. The counterweights and manual drive were then removed.

The safety drive system was then electrically checked. The rods were driven up and down electrically. Then, with the rods up, a simulated period trip scrammed the safety rods. The system operated normally.

Possible binding of the eleven control rods in the reactor grid was checked by raising each rod manually 51 in. All were raised and lowered easily without indication of any binding. Control rod drives Nos. 7, 8, and 9 were installed. Check of control rod drive grippers and sensing rod functions for all twelve rods was then completed.

Drop times of the control and safety rods were obtained, both for the "flow" and "no-flow" conditions. The following table gives satisfactory results of the test:

Control Rod No.	Drop Time (without flow, msec)	Drop Time (with flow, msec)
1	225	240, 250
2	210	240, 242
3	230	250, 257
4	220	250, 246
5	215	240, 240
6	220	235, 250
7	220	240, 240
8	230	240, 250
9	225	250, 250
10	225	250, 245
11	230	250, 250
12	258	295, 285
Safety rods	998, 1000, 835, 950	700, 680

4. Inspection and Repair of Evaporator 702

In preparation for hydrostatic testing of the EBR-II steam generator, after installation of the new check valve in the feedwater line had been completed, chromate-treated water (approximately 1400 ppm CrO_4, pH about 9) was drained from the steam generator. This water had been in the evaporators and superheaters for wet layup since November 21, 1964, while the steam drum was empty for inspection and for installation of the new check valve in the feedwater line. After draining, the entire steam generator was filled with demineralized feedwater and drained again for removal of most of the residual chromate. Water drained from steam generator contained 210 ppm CrO_4. It was then filled with demineralized feedwater containing approximately 2000 ppm of morpholine (pH around 10).

Before hydrostatic testing, water was found in the air space between the water and sodium tube sheets of evaporator 702, indicating that a leak in

the tube sheet or tubes existed. Testing with a hydrostatic pressure of 2250 psig confirmed the leak but did not result in a drastic increase in leak rate.

The steam generator was drained to permit repair of evaporator 702. Following draining, evacuation was started by means of the air ejectors, as a means of drying the steam generator surfaces. After two days, the riser pipe was cut and rigged away from the top of the evaporator. Water was standing on the tube sheet to the level of the tube tops, about 3/8 in. above the tube sheet surface. There was a large accumulation of mill scale on the tube sheet. It consisted of small thin pieces which apparently had flaked off pipe walls and, possibly, internal surfaces of the steam drum. At the recirculation rate of boiler water through the evaporators, there apparently is not sufficient velocity and turbulence to suspend these pieces and carry them out of the evaporator. This mill scale might have been on the tube sheet since chemical cleaning of the steam generator in August, 1962 (having escaped dissolution by the cleaning reagent). It might also have accumulated during service, being transported into the steam generator with feedwater from piping which was not chemically cleaned, or migrating from the steam drum.

A pinhole leak in a tube-to-tube sheet weld was located by soap bubble testing of the tube sheet area and confirmed by dye-penetrant test. The leak was welded shut. Helium leak testing of the evaporator was in progress.

Examination of eight tubes in evaporator 702 with a borescope showed them to be covered uniformly with a thin, loosely adherent film of black magnetic oxide. The upper portions of some tubes also contained whitish, water-soluble "stains" which looked like deposits of boiler water solids.

Six tubes were inspected to a depth of about $10\frac{1}{2}$ ft from the tube top, the maximum depth attainable with the borescope used. Two other tubes were inspected to a depth of about $2\frac{1}{2}$ ft.

There appear to be numerous shallow "pits" in all of the tubes inspected. Although it was very difficult to estimate pit depth from the borescope image, the maximum depth was estimated to be less than 10 mils and, for the majority of the pits, less than 1 mil. In many cases, the "pit" appeared to be a break or discontinuity in the adherent oxide film on the tube surface. The largest pit observed appeared to be about 1/8 in. in "effective" diameter (being irregular but roughly circular).

Many longitudinal surface irregularities were observed also. These may have resulted from the tube-forming operations.

More pits were observed in the first 3 ft of the tubes than farther down. This may be related in some way to tube wall temperatures and steam bubble formation.

5. Maintenance and Modification

The guide tube in the auxiliary plug hole on the small rotating plug was removed, and the modified auxiliary gripper plug was installed in its place. This plug is now supported on springs which will be equipped with limit switches to detect binding between the lower end of the plug and the reactor vessel cover. The reactor vessel cover drive was reinstalled after the control rod drives were in place. Cover-drive screw-synchronization devices were modified, relocated, and installed at the bottom ends of the lifting screws.

Thirteen outlet thermocouples in the reactor vessel cover had been shorted by sodium leakage. Twelve were replaced with stainless steel-clad thermocouples. One cannot be installed because of difficulties encountered in insertion.

Modification of the secondary sodium pump control was completed and checked. The system is completely operable. Further changes to make it fail-safe are being studied.

The secondary sodium plugging loop was rewired with heating cable, and the loop has been restored to service.

The electrical work for the secondary sodium flow differential pressure cell modification is essentially complete. Heating of the cell and associated piping will be controlled from a temporary control panel located on the main floor of the boiler wing.

During tests, it was noted that one coolant passage of the No. 2 secondary recirculating pump was almost completely plugged. The passage is being cleaned.

An experimental differential pressure (dp) cell was installed in parallel with the existing dp cell on the main secondary sodium flowmeter. Valves were also installed to permit zeroing these cells while the system is in operation.

An alarm switch and a limit switch for the new manual vent valve were installed in the emergency airlock. The airlock alarm system was modified to include these items.

A check valve was installed in the steam-generator feedwater line in the Sodium Boiler Building. The welds were inspected radiographically and hydrostatically tested at 2250 psig. The installation is ready for service.

New trim for the feedwater control valve, intended to improve control significantly at low plant loads, arrived, was reassembled, and is ready for service. It is hoped that finer control of feedwater with the motor-driven pump in service will result from this modification.

6. Fuel Cycle Facility

a. Argon and Air Cells

(i) Cell Atmosphere. Since the last entry into the Argon Cell, approximately one year of highly satisfactory operation in the inert atmosphere has been experienced. At differential pressures of 2-3 in. of water below atmospheric, inleakage of air has typically been held to 0.2-0.3 cu ft/hr, and the purity of the atomosphere has been maintained in the ranges of 30-60 ppm oxygen, 25-50 ppm water vapor, and about 5% nitrogen. The typical consumption of argon gas, including that required for purging of transfer locks, has been about 3500 cu ft/wk.

(ii) Shutter Drive Units. Window-shutter drive units continue to cause difficulty by failing to open or close the shutters. It appears that the sliding shoe at the base of the shutter tends to gouge the metal wall strip and the drive torque requirement becomes excessive. It is proposed to install ball-bearing rollers to reduce this problem.

(iii) Correction of Manipulator Failure. The failure of the EBR-II Argon Cell manipulator No. 4, mentioned in the previous monthly report (see Progress Report for January 1965, ANL-7003, p. 28), was a result of a short in the 64-pin connector on the top end of the manipulator feed cable. Examination of the connector showed that a portion of the insulating material was severely carbonized, presumably as a result of arcing between adjacent conductor pins. This arcing is attributed to the poor dielectric strength of argon. A similar failure[1] occurred about a year ago on an identical connector for Argon Cell manipulator No. 2.

The insert in this connector has a National Electric Code (NEC) rating of 250 V ac or dc. The maximum voltage of any single circuit for the manipulator is 140 V dc, with higher voltages occurring as a result of switching transients. The nominal conductor spacing in the insert is 1/16 in., and this spacing is apparently not adequate for application in an argon atmosphere.

To eliminate the connector failures, the connector inserts will be changed on all six manipulator cables for the Argon Cell. The new inserts will have a conductor spacing of 1/8 in. and a NEC rating of 600 V. The revised connectors will have only 22-pin conductors. The 54 wires in the cable (there are three or more wires for each of 17 circuit sides) will be consolidated into 18 conductors and the 18 conductors will be soldered to the new connector. The increased conductor spacing in the new inserts should prevent arcing.

---

[1] Chemical Engineering Division Semiannual Report, January-June, 1964, ANL-6900, p. 109.

decanned elements will be passed through the pin-processing station for redetermination of diameter, length, and weight.

e. Preparation of Additional Unirradiated Fuel Elements

(i) Melt Refining. Three additional 9- to-12-kg ingots of fuel alloy were cast from scrap fully enriched uranium plate, material of 1.44% enrichment, and fissium elements. Pouring yields ranged from 89.0 to 90.3%, the low yield being attributed to the highly oxidized condition of the fully enriched scrap. Two skull oxidations were also completed.

(ii) Injection Casting. Four injection casting runs were carried out with 11.2- to-11.7-kg unirradiated alloy charges. In three runs, the average weight cast per mold ranged from 65 to 84 g (compared with a nominal weight of 68 g per 12.4-in. casting). The low yield of 65 g/casting probably resulted from a heavy dross layer accompanying the ingot, which had been prepared from highly oxidized scrap. Examination of the mold pallet indicated that the dross had resulted in metal starvation to clusters of five and six molds.

(iii) Pin Processing. Castings from the first injection-casting run described above were passed through the pin-processing machine for demolding and measurement. Of 94 pins processed, 69 were accepted. The principal cause for rejection was porosity as detected with the eddy current device. A recent improvement in this system has resulted in significantly increased sensitivity and simpler interpretation. In the original design, only the coil-impedance change was recorded, and surface and internal defects could not be differentiated. By providing for simultaneous recording of phase angle, which differs for surface and internal defects, differentiation is readily made by comparing the two traces.

(iv) Assembly and Welding. Thirty-two unirradiated elements were assembled and welded, and are awaiting leak detection. Alignment problems resulting in high leak test rejection rates with the magazine-fed element welder have prompted the design and construction of a manipulator-fed single-element welder. Tests of this unit are now being made. Pin alignment and positioning, as well as electrode gapping and replacement, appear to be much simpler with the single-unit device.

B. FARET

1. General

Progress on the various design packages of Title II beyond that reported previously (see Progress Report for January 1965, ANL-7003, pp. 32-33) is as follows:

Package III - Liquid Metal Heat Exchangers - Signed drawings and specifications have been received from the Architect-Engineer. These are being reviewed for final detail checking prior to signature by ANL and the AEC, and return to the Architect-Engineer for reproduction and distribution.

Package IV - Liquid Metal Pumps - Signed drawings and specifications for this package have been issued to the Laboratory for signature by ANL and the AEC.

Package V - Control and Instrumentation - This package is being reviewed by the Laboratory. A significant number of comments have been returned to the Architect-Engineer. Review on a high-priority basis continues.

Package VI - Special Piping Materials and Valves - This package is in the same category as Package IV - Liquid Metal Pumps.

Package VII - Special Early Procurement Items - This package is in the same category as Package IV - Liquid Metal Pumps.

Package IX - General Design - This package contains the bulk of the Architect-Engineer Title II design work. Review is continuing on material which has been submitted recently. The entire package is scheduled for final issue at the end of March, and the material still not on hand is related primarily to the liquid metal systems, the cell, and the argon cooling system. This package is being reviewed on a high-priority basis.

Based on a review of the Title II design as of the initial issue of design Package IX, the following significant changes to the Title II design have been made:

(a) The blowers for the argon cooling system are being relocated so that they will be in the vault.

(b) Concrete for the cell wall has been changed from magnetite to ordinary concrete.

(c) Criteria for the cavity seal design have been revised to allow use of a dust barrier instead of a total seal between the cavity and the vault.

(d) All hot traps and one primary system cold trap, together with one plugging meter and associated equipment, have been deferred for future installation.

(e) Considerable simplification in the plant-control system, including deletion of the six automatic control modes, has been effected.

(f) One of the two argon-purification units has been deleted.

(g) Considerable simplification in the arrangement and control of the pipe electrical heating system has been effected.

(h) Further design simplification has been directed throughout the plant in connection with general services and utilities related to such things as outside lighting, fences, heating and ventilating equipment, and equipment assistance.

The remaining ANL reviews of Bechtel's Title II design drawings and specifications are not expected to produce many additional significant design changes of this type. They should rather be generally confined to checking for follow-up details necessary for approvals to release drawings and specifications.

2. Cell Modification

Since it is thought essential that control drives be accessible for inspection and adjustment "in place" and preferably without the necessity for personnel to wear air packs in an argon atmosphere, a thorough review of the in-cell requirements was made. There are also certain difficulties to operating the drives in the cell such as the routing of control cables necessary for the drives; this would be difficult to accomplish, and cable connections would be difficult to make and break within the cell. Further, the operation of the control drive would require development of electrical components for satisfactory operation in argon atmosphere.

Efforts have been made to isolate the control drives by means of various enclosures, so that access would be possible while maintaining an argon atmosphere in the cell. The difficulty with these schemes is the lack of a solution for the movement of the enclosures within the cell, so that the reactor head and the control drives could be lifted frequently for the installation and removal of fuel subassemblies.

A system has now been designed which will permit the control drives and the reactor vessel cover to be in an air atmosphere with manual access for minor adjustment. The use of this system has eliminated the cable-connection problem and also permits control-drive replacement without having to enter the argon cell. This is accomplished by means of an impervious fabric bellows, together with an upper cell structure (see Figure 1). The upper cell would normally contain air, while the main cell contains argon. Removal and repair of control drives may be made while the reactor cover is in the upper position. The in-cell equipment can then be operated in a normal manner while the cover is in the upper position to permit access of fuel-handling equipment to the core for refueling.

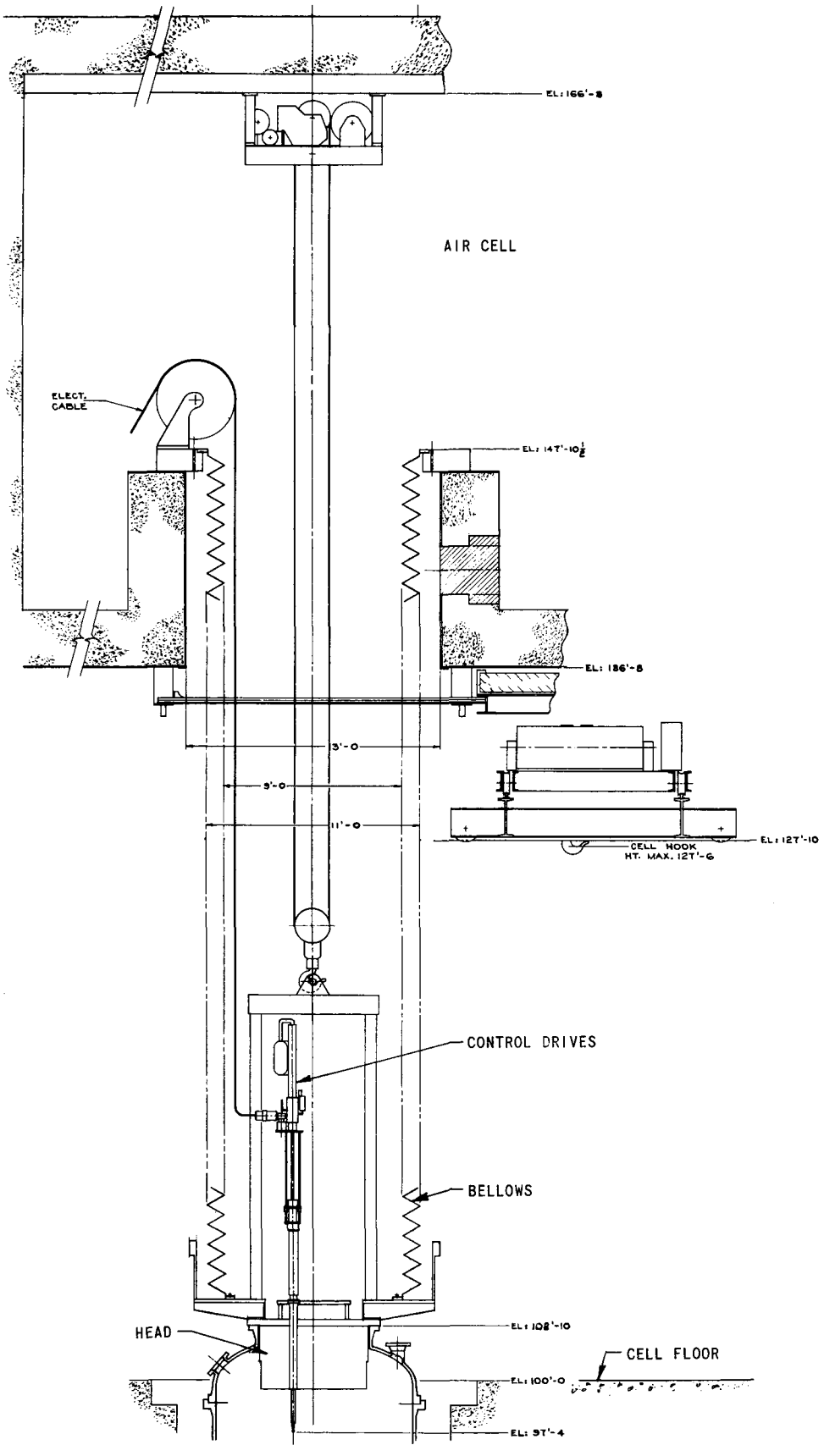

Figure 1. Cell Modification for Control Rod Drives

A manufacturer has been located who has the essential experience for fabrication of the bellows. Sample materials have been received, and a sample bellows section has been fabricated. A test setup is in preparation to measure permeability of moisture and gases through the fabric. Materials of interest are neoprene, rubber, and hypalon. Another test apparatus is being designed for the testing of a full or smaller scale section.

The introduction of a rectangular air cell on top of the heretofore rectangular FARET cell places additional requirements on the FARET containment system. The height of walls and slabs must be almost doubled. The existing wall thicknesses are not sufficient to absorb the increased moments and stresses. In order to avoid drastic and expensive changes in the design at this late stage, an approach of tying the base of the protruding air cell with a stiffening rectangular box frame was devised. This box frame, at approximate baseline elevation of 140 ft, makes up for the continuity in the ceiling originally present in the cell; it provides a stiff base for the new air cell; it cuts by almost a factor of two the heights of the subject slabs and frames, thus resulting in a stress reduction by a factor of almost four. Study is being made of the most effective way to provide this box frame. A reinforced concrete section, a post-tensioned beam section, a steel box section, and their respective combinations are being considered.

3. Shielding Windows

The hydraulic pressure test of a test slab (29 in. x 44 in. x $8\frac{1}{2}$ in. thick, see Progress Report for June 1964, ANL-6912, pp. 50-51) of glass has been completed successfully. Hydraulic pressures were attained up to 160 psi, corresponding to a maximum calculated bending stress of about 900 psi.

The maximum stress at the center of the glass slab, derived from strain-gauge data, was in the range from 850 to 925 psi. During the time the test fixture was pressurized, no liquid leak or loss of pressure was noted. Also, an initial leak test with compressed air at 6 psig failed to indicate any detectable leakage over a 5-day period. A final leak test with helium gas to a pressure of 6 psig (following the hydraulic test) indicated an average leak rate of 0.03 scf/day over a $12\frac{1}{2}$-day period.

The use of heavy glass slabs of large area as a pressure sealed membrane appears to be practical when using machined steel surfaces and a glass slab for gasket surfaces which are flat within 0.005 in. Gaskets of Koroseal 116, 1 in. wide x 1/8 in. thick, were found satisfactory. Since only simple flat gasket surfaces were used for the high test pressure of 160 psi in the experiment, no specially machined grooves or channels are needed for the FARET application at 31 psi.

4. Reactor Vessel

The core-support structure, which initially employed three supporting plates to subdivide the low- and high-pressure regions, has been redesigned to include two plates with dimensions similar to those of the EBR-II. This change enables the use of similar inlet flow adapters to the fuel subassemblies. The low-pressure region is still maintained by means of a separate ellipsoidal chamber below the lower support grid. This type of construction was found to reduce the complexity of the support grid and should result in a cost reduction.

Another study has been made to include the graphite shielding necessary for neutron attenuation in the reactor vessel to take advantage of cooling by the sodium. This arrangement has necessitated the placement of the inlet coolant downcomers close to the outside of the reactor vessel to enable four rows of EBR-II-sized graphite cans to be installed. The arrangement of the shielding inside the reactor vessel and the downcomers is shown in Figure 2.

The new arrangement has made it necessary that the tempering coils and the auxiliary distribution header be placed in the bottom portion of the reactor vessel.

5. Core Design

Because the first core for FARET will now be a core for fuel investigations rather than a zoned core for Doppler-broadening investigations, a new reference core has been designed to consist of 61 fuel assemblies with a core height of approximately 20 in. The basic core volume is 93 liters. Various subassembly designs, utilizing oxide, carbide, or metal fuel, can contain mainly 37 and 61 fuel pins per subassembly. The basic parameters for this reference core and a comparison with reactor criteria from 1000-MWe studies are shown in Table I. (See item I.C.1 for a discussion of the FARET Core I critical being performed on ZPR-III).

With this reference core the FARET facility should be particularly adapted to testing the performance capability of fuels as the initial phase of the FARET program. The core support grid has been provided with 301 places for loading elements. Thus, the number of elements that are available in the reflector zone should permit various irradiation possibilities, in addition to those of the core, so that irradiation of structural materials involving variations of power and flow conditions may be incorporated, and also the utilization of planned loops. With loops, irradiation and safety experiments leading to the release of fission products or the deliberate failure of the fuel may be contemplated.

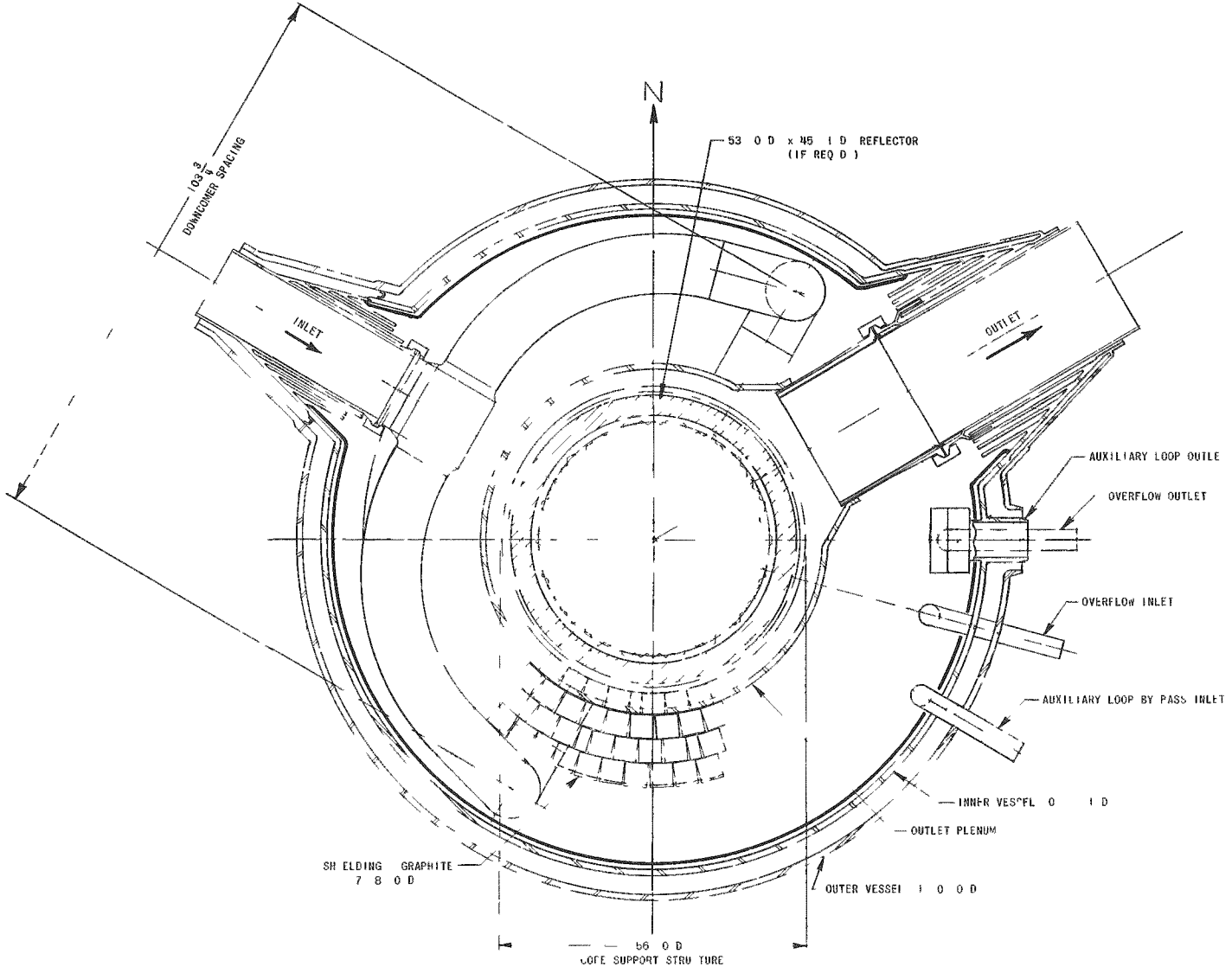

Figure 2 Arrangement of the Shielding inside the Reactor Vessel and the Downcomers.

Table I. Comparison of Selected Reactor Data

Parameter	1000-MWe Studies				EBR-II	FARET Subassemblies (Illustrative)		
	AC	GE	CE	WE				
Fuel	Oxide	Oxide	Carbide	Carbide	Metal	Oxide	Carbide	Metal
Pins per Subassembly	-	-	-	-	91	37	37	61
Active Height, in.	48	24	30	75	14	20	20	20
Fuel Clad OD, in.	0.30	0.25	0.30	0.30	0.174	0.28	0.28	0.22
Clad Thickness, mils	28	15	11	10	9	20	20	17
Power Density (avg), kW/ℓ	280	365	690	310	735	405	605	535
Power Density (max), kW/ℓ	430	790	1060	710	1250	583	875	770
Linear Power (max), kW/ft	13.1	22.7	43.7	29.1	12.4	14.4	21.6	11.5
Linear Power (avg), kW/ft	8.6	10.4	28.1	12.0	8.1	10	15	8
Sodium Velocity (max), ft/sec	~20	13.6	23.4	31.8	23.8	16	24	23
Sodium ΔT, °F	250	300	250	220	200	240	240	240

Another basic plan has been included in the processing or transfer of core subassemblies. The core subassemblies are currently being redesigned so that the EBR-II method of handling fuel into the Fuel Cycle Facility can be utilized in the FARET process. The handling of items such as scrap containers will utilize equipment identical with that used in the EBR-II facility.

6. Control Drives

The reservoir of sodium for the bellows seal (see Progress Report for January 1965, ANL-7003, pp. 34-37) reached the operating temperature of 1150°F. To date the bellows seal has successfully completed 1200 cycles. Each cycle consists of moving the drive shaft with the bellows up and down through a 36-in. stroke at a speed of 10 in./min.

7. Fuel Assembly Sodium Flow Test Loop

The casting for the 800-gpm pump volute has been made by the Esco Foundry of Portland, Oregon. Five inclusions, now being repaired, were found upon radiography. ANL and Byron-Jackson inspectors must approve and accept the casting. The B-J schedule calls for casting delivery the last of March, 1965.

About 10% of field welding of prefabricated pipe lengths has been completed. Vessel lagging is progressing. Power electrical work is nearly completed.

The preliminary test of the Baldwin-Lima-Hamilton high-temperature full-bridge gauges is nearing completion of five gauges initially available, two were lost in handling operations; the leads broke off one gauge, and the cement cracked in the other. The third gauge failed at 450°F, leaving two gauges in operation at the present time. One of these appears to be only partially temperature-compensated. It appears that high-temperature strain measurements will require further attention.

8. FARET Subassembly Cutoff Machine

General design requirements for the fuel subassembly cutoff system have been completed (see Table II). Basically, the core subassemblies will be cut and separated so that the existing EBR-II components and facilities can be utilized to handle the cutoff portions. Conceptual design of the machine and its installation is nearing completion. This includes drawings covering the design of tubing cutters, instrument lead cutters, electrical and pneumatic service connections and provisions for remote disassembly.

Table II. Subassembly Cutoff Criteria

Machine Orientation	Vertical
Viewing	Through cell window and mirrors
Control	From control station oustide cell
Subassembly Types Handled	Fuel, instrumented, reflector, control, source, and control rod tubes
Cutting Method	Roller tube cutter type (EBR-II type)
Cutter Actuation	Pneumatic, using compressed argon
Cooling	Forced argon (1000 W)
Positioning	Electric-motor-driven change hoist device
Position Indication	Mechanically coupled dials inside cell viewed through window
Cutting Debris	Picked up by suction and filter as part of cooling system

The machine has the capability of cutting the hexagonal tubing of a subassembly at designated points, cutting a number of instrument leads, and removing 1000 W of decay heat. Handling of scrap and replacement of cutters will be accomplished by an integrally mounted transfer arm. All major subassemblies of the machine will be designed as plug-in units to permit removal from the cell by means of the in-cell crane. It is planned to make repairs and adjustments outside of the cell.

C. General Fast Reactor Physics

1. ZPR-III

The ZPR-III Assembly 46 is intended to provide critical data useful in the design of the first core loading of FARET. The radial and axial reflector regions in the assembly approximate in composition and geometry those intended for FARET. Figure 3 and Table III provide the details of these reflectors.

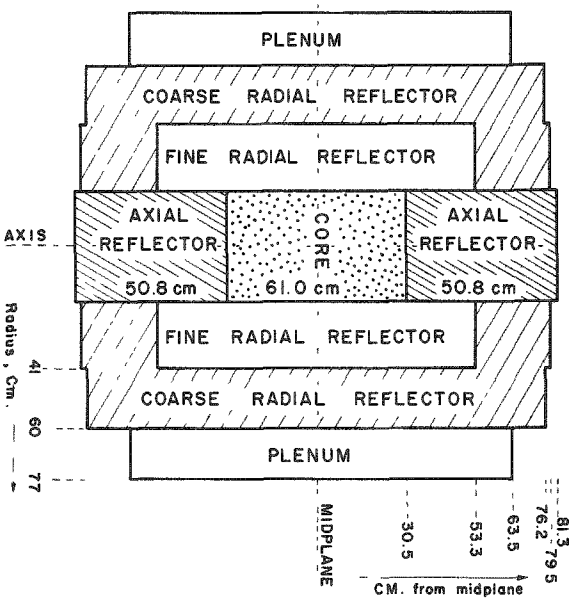

Figure 3

Axial Schematic of ZPR-III Assembly 46

Table III. Compositions of Reflector Regions of ZPR-III Assembly 46

	Composition, g/cc, in Region			
Material	Axial Reflector	Fine Radial Reflector	Coarse Radial Reflector	Plenum
Fe	3.115	4.388	6.873	0.413
Cr	0.779	1.097	0.103	0.103
Ni	0.433	0.610	0.057	1.874
Na	0.323	0.081	-	-
Al	-	0.137	-	0.620
Mn	-	-	0.052	-
C	-	-	0.013	-

The first core loaded into the assembly, designated core 46A, simulates a carbide-fueled system with a composition of 36 v/o fuel (PuC-UC), 38 v/o sodium, and 18 v/o steel. In the fuel, the atom ratio of uranium to plutonium is 5.5:1, with the uranium enriched to 45.7% in U^{235}. Table IV gives the core composition. This fuel composition was loaded into the ZPR-III drawers to a depth of 12 in. (30.5 cm) in each half, making the core length 24 in. (61 cm). The just-critical loading for this core 46A was found to be 60.3 fuel drawers with a volume of 56.4 liters. This value provides the average core radius of 6.76 in. (17.15 cm) and critical fuel loading of 36.7 kg plutonium plus 91.0 kg U^{235}. The volume obtained is smaller than desired for proper correlation with FARET design, and no further experiments were done.

Table IV. Compositions of Carbide-simulation Cores in Assembly 46

	Core 46A		Core 46B	
Material	g/cc	v/o	g/cc	v/o
Pu[a]	0.651	3.5	0.651	3.5
U^{235}	1.614	8.6	1.318	7.0
U^{238}	1.939	10.2	2.245	11.8
C	0.222	13.4	0.222	13.4
Steel[b]	1.361	17.4	1.361	17.4
Na	0.323	38.5	0.323	38.5

[a] Isotopic composition 95.03 w/o Pu^{239}, 4.56 w/o $Pu^{240+242}$, and 0.42 w/o Pu^{241}.
[b] Type 304, nominally 72 w/o Fe, 18 w/o Cr, and 10 w/o N.

The second core composition loaded, designated 46B (see Table IV) was obtained by reducing the uranium enrichment in the 46A core design. The fuel (equivalent to 36 v/o PuC-UC) still contained 5.5 atoms uranium per plutonium atom, but the uranium enrichment was changed from 45 7 to 37.3% U^{235}. With the same 12-in. core length in each ZPR-III half, the just-critical loading for core 46B was found to be about 73 drawers, with a volume of 68.3 liters. Correspondingly, the average radius is then 7.53 in. (19.1 cm), and the fuel loading is 44.4 kg plutonium plus 90 0 kg U^{235}.

Measurements of spectral indices at the center of core 46B have been carried out. Included in the experiments were the relative fission

rates of U^{235}, U^{238}, U^{234}, U^{236}, Pu^{239}, and Pu^{240}. Also, measurements of the ratio of U^{238} capture to U^{235} fission were made. Control rod calibrations and determinations of fuel worth at the core edge are in progress.

2. ZPR-VI

The sodium-void coefficient was measured in a sector representing one-eighth of the total core in Assembly No. 3 of ZPR-VI. The measured reactivity change after voiding the sector was -2.77 Ih/kg, in good agreement with the calculated sodium-void coefficient for the total core of -2.86 Ih-kg.[3]

After this measurement, the core was modified by introducing a 39-cm-dia dilute blanket zone in the center of the axial U^{238} reflector in both halves in order to determine the influence of the reflector composition on the sodium-void coefficient and other reactor parameters. The atomic densities in this zone (in units of 10^{22} atoms/cc) were: U^{238}, 1.232; U^{235}, 0.0025; stainless steel, 1.475; carbon, 1.29; sodium, 0.791. The introduction of the dilute reflector zone produced a reactivity increase of +13 ± 3 Ih.

The reactivity change was calculated to be +61 Ih if the entire axial reflector composition had been changed to a dilute composition. This corresponds to a reduction in critical mass from 850 to 830 kg, using the fuel worth at the radial edge.

With the dilute blanket zone, the sodium-void coefficient was measured for several regions on the core axis, with different axial dimensions and a diameter of 28 cm. The measurements in the core were also made with all the sodium removed from the dilute blanket behind the region of measurement. The sodium-void coefficients became more negative as the blanket was diluted. The calculated values, which are generally more negative than the measured values, indicated a similar dependence on the blanket composition (see Table V).

Table V. Sodium-void Coefficients for Different Blanket Compositions

Regions		Measured Values (Ih/kg)				Calculated Values (Ih/kg)		
		Heavy	Light Blanket			Heavy	Light Blanket	
Inner[a] Boundary	Outer[a] Boundary	U^{238} Blanket	With Na	Without Na[b]	Estimated Uncertainty	U^{238} Blanket	With Na	Without Na[b]
				Core				
0	7.62	-0.18	-0.3	-0.6	0.3	-1.67	-1.68	-1.99
15.24	25.4	(-5.9)[c]	-6.38	-6.82	0.2	(-6.3)[c]	-6.8	-7.66
0	25.4	-3.48	-3.57	-3.92	0.1	-4.03	4.37	-4.98
				Blanket				
25.4	33.0	-	-4.54	-	0.2	-	-5.44	-
25.4	55.8	-	-2.90	-	0.1	-	-2.97	-

[a]Distance from midplane, in cm.
[b]For all measurements under this heading the sodium in the blanket was removed permanently while the sodium-void coefficient in the core was measured.
[c]These values were estimated from the results for two smaller regions, extending from 15.24 to 20.32 cm, and from 20.32 to 25.4 cm.

[3]All calculations reported in this section were made with the one-dimensional diffusion code MAIM-VI and cross-section set 224.

Table VI shows the results of axial fission traverses taken with U^{235} and U^{238} foils. The reflector fluxes are significantly higher for the dilute blanket, and this is probably the cause for the increase in reactivity. There is no great difference in the U^{238}/U^{235} fission ratios. The measured and calculated fission rates are in good agreement.

Table VI. Axial Fission Traverses for Different Blanket Compositions

Distance from Midplane (cm)	Fission Rates in U^{238}[a]		Fission Rates in U^{235}[b]		U^{238}/U^{235} Fission Ratio[b]	
	Heavy Blanket	Light Blanket	Heavy Blanket	Light Blanket	Heavy Blanket	Light Blanket
			Core			
0 meas	1.000	1.000	1.000	1.000	0.0346	0.0346
calc	1.000	1.000	1.000	1.000	0.0355	0.0357
14.6 meas	0.845	0.844	0.859	0.865	0.0340	0.0338
calc	0.822	0.834	0.856	0.868	0.0341	0.0343
24.8 meas	0.457	0.475	0.601	0.677	0.0262	0.0242
calc	0.452	0.478	0.603	0.687	0.0265	0.0249
			Blanket			
29.2 meas	0.178	0.262	0.426	0.600	0.0145	0.0151
calc	0.197	0.283	0.423	0.612	0.0165	0.0165
32.4 meas	0.105	0.172	0.321	0.530	0.0133	0.0112
calc	0.106	0.193	0.322	0.545	0.0117	0.0126

[a]Normalized to unity in the core center.
[b]The fission ratios measured by foils were calibrated to absolute Kirn-counter measurements which had been performed in the center of the core.

After these experiments, Assembly No. 3 was shut down. The reactor was unloaded. The facility is being prepared for a 3000-liter zoned-core carbide assembly.

3. ZPR-IX

Work has been completed on ZPR-IX, Assembly No. 6. The measured worth of edge fuel was found to be 17.6 Ih/kg U^{235}, to be compared with the calculated value 15.9 Ih/kg. The experimental cylindrical critical mass was found to be 453.5 kg. The core length was 61.26 cm, the critical radius 36.62 cm (L/D = 0.836), and the critical volume 258.1 liters. In order to compare calculated and measured values of critical mass and volume in spherical geometry, the measured values were adjusted accordingly. A net addition of 6.8 kg U^{235} was made to allow for heterogeneity, cylindrical boundary irregularity, and central gap, increasing the critical mass to 460.3 kg of U^{235}. If a shape factor of 0.931 is used, the equivalent spherical critical mass is reduced to 428.6 kg and the volume to 243.9 liters, which may be compared with values of 444.6 kg and 253.2 liters calculated from a sixteen-group one-dimensional spherical diffusion calculation. From a Rossi-alpha measurement, the prompt lifetime was estimated to be 154 nsec, as compared with a calculated value of 122.0 nsec.

The central reactivity worths of a number of materials were measured and calculated (see Table VII). The central U^{238}/U^{235} fission ratio was radiochemically measured as 0.0443, to be compared with a calculated value of 0.0488.

Table VII. Central Reactivity Worths (Ih/kg)

Material	Observed	Calculated
U^{235}	148	141.0
Pu^{239}	252	234.4
U^{233}	266	245.0
U^{238}	-3.4	-3.2
B^{10}	-2065	-1920.0
W	-10.6	-11.0
Re	-39.1	-54.7
Al	-3.0	4.2
C	8.6	31.4
Au	-20.1	-

Central worth measurements were also made of some samples of polyethylene (14.3 w/o hydrogen). The results (see Figure 4) varied between 2.6 and 3.75 Ih/g of hydrogen, and are to be compared with calculated worths of 2.50 Ih/g using fission-spectrum-weighted cross sections, and 2.93 Ih/g using 1/E-weighted cross sections for infinitely hydrogen-diluted samples. Samples smaller than a total weight of 15 g were composed of polyethylene strips enclosed in aluminum cans; larger samples were solid polyethylene blocks drilled out to the required weight.

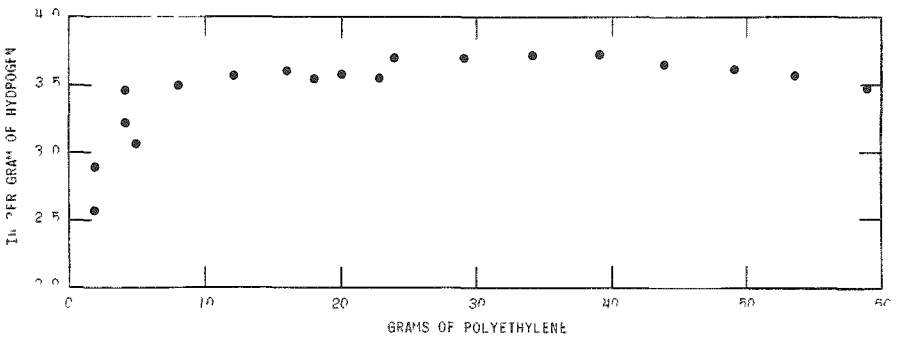

Figure 4. Central Worth Values for Polyethylene Samples of Various Weights. Samples smaller than 15-g total weight were composed of polyethylene strips enclosed in aluminum cans; larger samples were solid polyethylene blocks drilled out to the required weight.

Central worth measurements were also made of samples consisting of mixtures of natural boron and Lucite powders. The worth of each sample per gram of boron (relative to 100% boron) is shown in Figure 5.

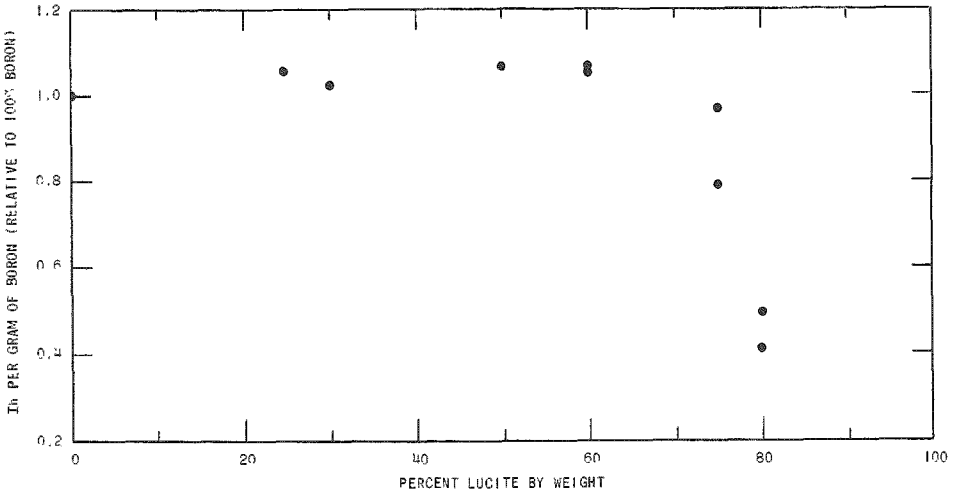

Figure 5. Plot of Central Reactivity Worths for Boron in Mixed Powders of Lucite and Boron vs. Fraction of Lucite Present

The gap worth was remeasured with the counter located inside (where the Rossi-alpha measurement was made) and behind the core. The results of the former measurement are shown in Figure 6 as plotted out by the DDP-24 computer. No significant differences were seen between these measurements and those previously reported. It is therefore concluded that this assembly has a much lower gap worth than Assembly No. 4.

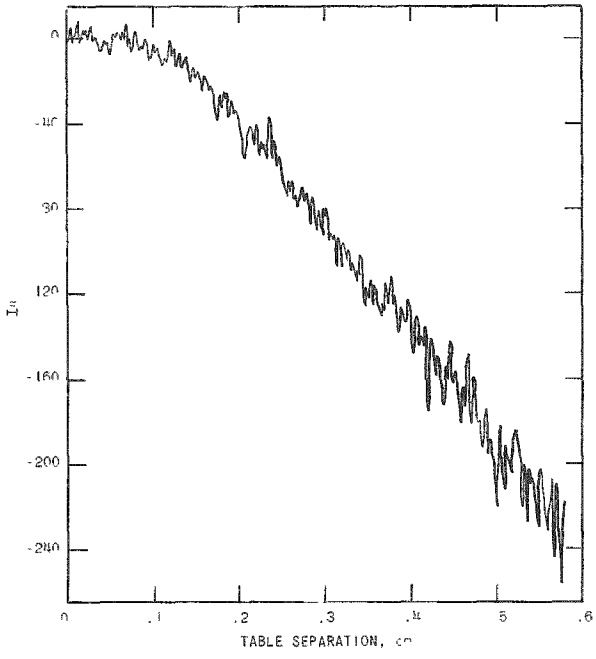

Figure 6

Change in Reactivity with Change in Gap in the ZPR-IX Assembly No. 6 as Plotted by the DDP-24 Computer Based on Data Furnished by a Counter Located inside the Core

4. ZPPR

The Title I report of the ZPPR Facility has been completed by the architect-engineer, Mason-Hanger, Silas-Mason Co., Inc., and was issued on February 16.

a. Reactor Bed and Tables. The bid package for the reactor bed and tables has been sent to prospective bidders. The due date on the bids is March 15.

b. Matrix Assembly. The details of the matrix tubes and drawers are being fixed. The inside dimensions of the matrix tubes have been fixed at 2.093 ± 0.004 x 2.193 ± 0.004 in. with a 0.040 ± 0.001-in. thickness. The matrix tubes will be 48 +1/16, -0 in. long.

The nominal lengths of both fuel and blanket drawers have been set at 23 in. The exact length will be determined by the space required for the spring to hold the core-mockup materials in place.

c. Reactor Fuel Design. One of the desirable characteristics in a critical facility is that the fuel expands upon heating and that the propagation of expansion along the fuel column act as a shutdown mechanism. Any fuel cladding, therefore, should be designed to avoid restraint of the expansion characteristics of the fuel.

Three types of fuel plates have been subjected to transient tests in TREAT to explore the expansion characteristics of some zero-power reactor fuel claddings. In all cases, the fuel was of depleted uranium (0.2% enriched).

One set of plates consisted of unclad, Kel-F-coated, uranium pieces from ZPR-III.

A second set of plates was made up of simulated SEFOR critical fuel plates, containing depleted uranium instead of the actual U:Pu:Mo alloy (see Table XI , p. 20, in Reactor Development Program Progress Report for January 1965, ANL-7003). Although measurements of the core meat and jackets of the two elements used in the experiment indicate a clearance of 0.007 in. before canning, X-rays of the finished fuel elements showed no clearances between the ends of the fuel and the cans.

The third set of fuel cans represented a stage of the developmental design in which the construction is simplified and, at the same time, clearances within the jacket are reduced. The cladding was a modified sodium can such as is used for mockups in ZPR-III and ZPR-VI (0.250 in. wide, 2 in. high, and 0.015 in. thick) with end plates pushed against the fuel during welding so that there is no clearance between the ends of the fuel

and the can. X radiography of the completed fuel plates confirmed that there were no end clearances. This design has about 3% void inside the can and essentially no dead space outside the can.

The test apparatus, fabricated to fit inside a TREAT transparent capsule, is shown in Figure 7. A cut-down ZPR-III drawer was fitted into the frame. Mockup pieces of aluminum were placed along each side of the test pieces to simulate an actual reactor drawer in its matrix tube. A linear transducer was adapted through a hole in one end of the apparatus to bear against the end of the fuel columns. The opposite end of the fuel column was bottomed against the drawer and test apparatus to prevent motion. One thermocouple was inserted into the meat of one of the test pieces and another attached to the cladding.

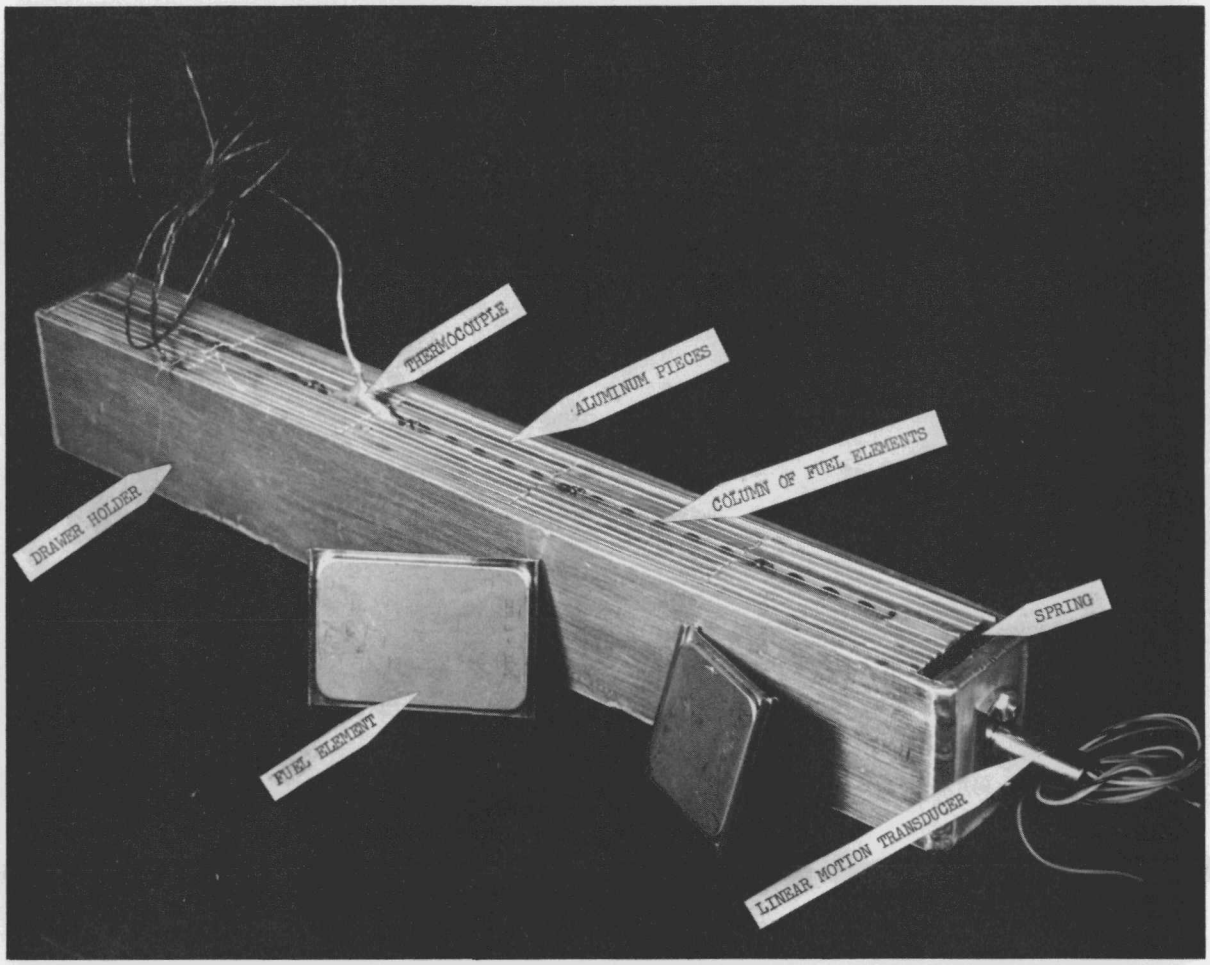

Figure 7. Apparatus for Fuel-expansion Test

The test apparatus was inserted into a TREAT transparent capsule and the whole installed into the reactor. The samples were irradiated during a TREAT reactor excursion, and continuous recordings were made of the outputs of the linear transducer and thermocouples.

The results of these experiments are shown in Figure 8. There is a delay in each case in the start of motion, due probably to clearances between the ends of the pieces.

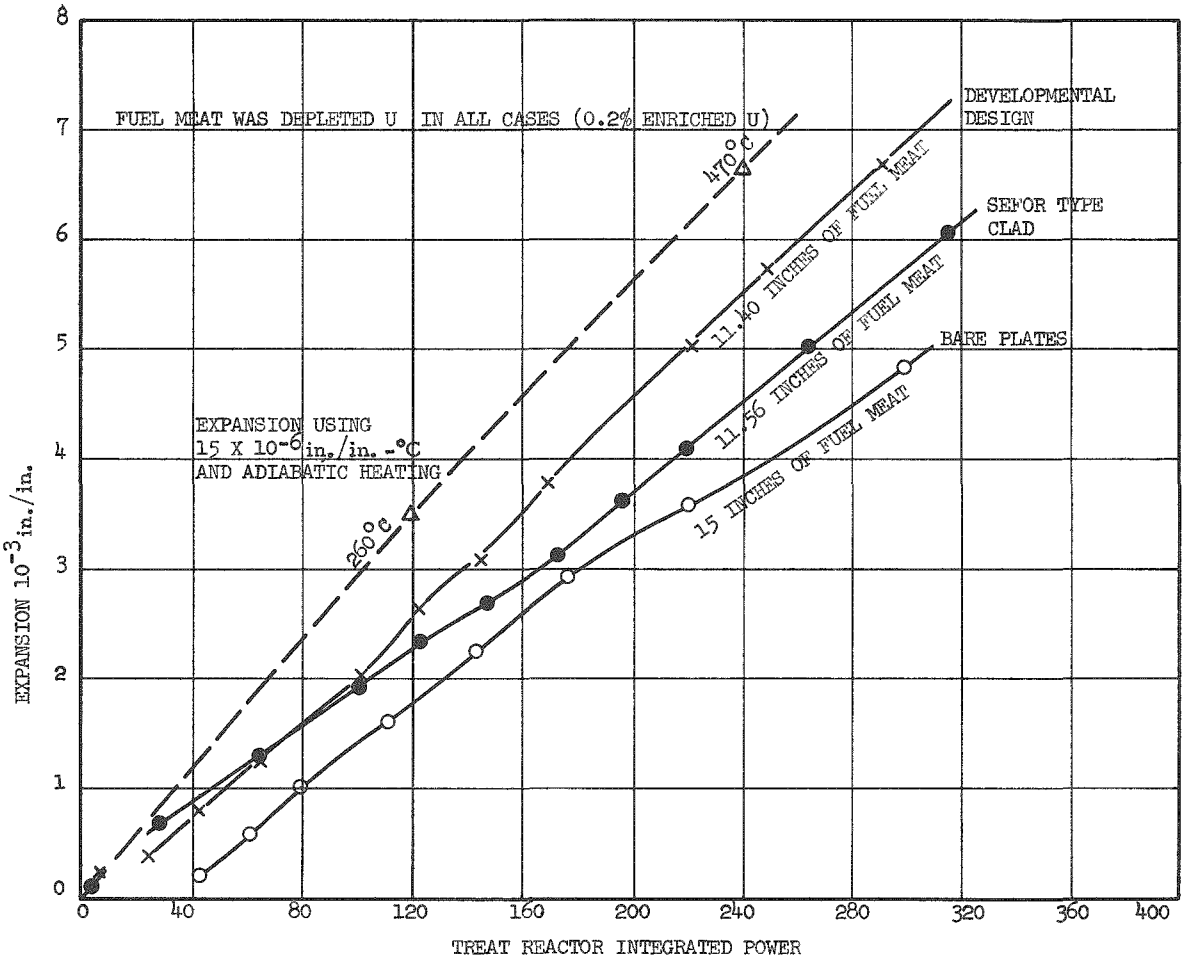

Figure 8. Transient Expansion Characteristics of Some ZPPR Fuel-cladding Designs

The theoretical expansion of uranium is plotted for comparison. The adiabatic temperature of the pieces was calculated from the heat capacity and a measured fission rate. The measured meat temperature appeared to be 15% low. A major part of this difference is probably due to heat losses during the transient. The measured temperatures are not shown, but an analysis of the data indicates a lag of the thermocouple response to the reactor integrated power.

These experiments indicate that expansion of the fuel columns can be relied upon as a shutdown mechanism. Further work on cladding of plutonium fuels for critical facilities is continuing. A major problem concerns the insertion of the fuel meat into the cladding and subsequent welding without contaminating the welds and the outside of the cans.

D. General Fast Reactor Fuel Development

1. Metallic Fuels

a. Improved Uranium-Plutonium-based Fuels. Of the several elements studied, titanium and zirconium were found to have the greatest promise for raising the solidus temperatures of U-Pu alloys. The pertinent properties of U-Pu-Ti and U-Pu-Zr alloys are being studied in an effort to develop metallic U-Pu-based fuels that melt at higher temperatures than do the U-Pu-Fz alloys in order to permit higher fuel operating temperatures and also result in a safer fuel in the event of an excursion. From physics considerations, titanium and zirconium are also the least undesirable of the elements studied.

Castings of these alloys in a range of compositions have been made by both top-pour chill casting into a copper mold and by injection casting into yttria-coated Vycor and quartz molds. In general the U-Pu-Ti alloy castings were readily machined whereas the U-Pu-Zr alloys were brittle and difficult to machine in the as-cast condition.

The compressive strength and ductility of a U-15 a/o Pu-40 a/o Ti (U-22.1 w/o Pu-11.8 w/o Ti) alloy casting have been determined as a function of temperature (see Table VIII). The alloy is extremely strong and, unlike comparable U-Pu-Fz alloys, retains an appreciable strength above 600°C. Although possessing little ductility up to about 400°C, the ductility is appreciable at and above about 500°C.

Table VIII. Compression Properties of U-15 a/o Pu-40 a/o Ti Alloy (As-cast Injection Castings)

Temp (°C)	Ultimate Compressive Strength (kg/mm^2)	Reduction in Length (%)
25	141	<1
405	71	<1
516	48	~10
618	34	>16*
717	11	>12

*The test was stopped when the specimen deformed continuously without an increase in load.

The expansion behavior of several alloys has been determined as a function of temperature to about 950°C in a vertical, quartz pushrod dilatometer. The data are summarized in Table IX.

Table IX. Dilatometric Data for U-Pu-Ti Fuel Alloys

Alloy Compositions (a/o) (w/o)	U-10.7 Pu-35.8 Ti U-15 Pu-10 Ti	U-15 Pu-40 Ti U-22.1 Pu-11.8 Ti	U-14 Pu-30 Zr U-17.2 Pu-14.1 Zr
Expansion Coef. x 10^6/°C (25°C to transformation)	20.3	16.9	18.2
Transformation Range, °C Expansion, $\Delta\ell$	750-848 1.09%	653-812 1.14%	596-665 0.58%
Expansion Coef. x 10^6/°C (Transformation to 950°C)	19.7	21.3	22.3

Fuel pins, 3.66 mm in diameter by 100 mm long, of a U-15 a/o Pu-35.6 a/o Ti alloy and a U-15 a/o Pu-30 a/o Zr alloy have been injection cast, inspected for defects by radiography, and submitted for irradiation testing.

The compatibility of the U-15 a/o Pu-40 a/o Ti alloy was checked against V-20 w/o Ti, titanium, zirconium, and stainless steel by the diffusion-couple method. The V-20 w/o Ti alloy has good compatibility whereas the others have poor compatibility.

The phase relationships and structure of U-Pu-Ti alloys in the composition range of fuel interest are being studied. The U-Ti system has a hexagonal compound, U_2Ti, which transforms to gamma U-Ti solid solution at 898°C. We have confirmed preliminary indications by Los Alamos[4] that plutonium replaces uranium in the binary compound and causes an expansion of the lattice. The solidus temperatures as determined by metallographic examination of quenched specimens of the ternary alloys are considerably higher than those of binary U-Pu alloys of the same uranium-to-plutonium ratio. X-ray diffraction studies as well as elastic-modulus determinations confirm the French observation[5] that the high-temperature body-centered-cubic gamma phase cannot be retained upon quenching.

An arc-cast U-16.67 a/o Pu-33.33 a/o Ti alloy, made of high-purity materials, was homogenized for one week at 1050°C and water quenched. Metallography gave no indication of incipient melting. The X-ray diffraction pattern showed all the lines of the hexagonal $(U,Pu)_2Ti$ phase with lattice parameters of $a_0 = 4.803 \pm 0.001$ Å, $c_0 = 2.850 \pm 0.001$ Å, and $c/a = 0.5885$.

[4]Schönfeld, F., to Kelmah, L. R., private communication, dated December 2, 1964.

[5]Boucher, R., and Barthelemy, P., Comparison of the Alloys U-Pu-Mo, U-Pu-Nb, U-Pu-Ti, and U-Pu-Zr, CEA-R2531, ANL-TRANS-138.

2. Development of Jacket Materials

a. Vanadium Alloys.

(i) Extrusion of V-20 w/o Ti (TV-20) Tube-Blanks. Following the development by the Argonne Metallurgy Division of methods of fabricating TV-20 and the selection of this alloy as a likely material for the jacketing of fast reactor fuels, industry was encouraged to participate in its production and fabrication development. TV-20 extruded bar stock, purchased from Union Carbide and extruded at Canton Drop Forge Company (see Progress Report for January 1965, ANL-7003, p. 14), has been inspected and analyzed by radiographic, ultrasonic, metallographic and wet chemical means.

Three billets for tube-blank extrusion were machined from some of the above extruded bar stock. The first billet stalled the press when extruding at an 11.4:1 reduction ratio at 1100°C. The billet was salvaged and recanned. All three billets extruded satisfactorily at an 8.5:1 reduction ratio at 1150°C. The extruded tube blanks have been dejacketed and are starting through secondary fabrication.

(ii) Thermal Expansion of TV-20 Alloy. The thermal expansion of TV-20 was determined over the temperature range 25-967°C at a heating and cooling rate of 2°C/min. The expansion curve is given in Figure 9 along with the calculated expansion curves of unalloyed titanium and vanadium derived from published mean values of the expansion coefficient.

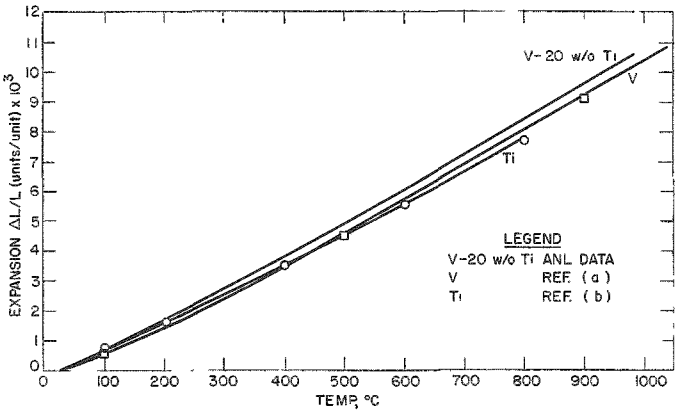

Ref. (a) Hample, C. A., Rare Metals Handbook, 2nd Ed. (1961), p. 635, Reinhold Pub. Corp. (London).

Ref. (b) Smithells, C. J., Metals Reference Book, 3rd Ed. (1962), Vol. 2, p. 697, Washington Butterworths (London).

Figure 9. Thermal Expansions of Titanium, Vanadium, and TV-20 Alloy

(iii) Creep of Tubular Specimens under Triaxial Stress. Creep tests of tubular specimens are being conducted under an internal gas pressure. In Figure 10 the tangential stress generated in the outer surface of a Type 304 stainless steel tube is plotted against the time for rupture. These results are in close agreement with rupture data generated at the Oak Ridge National Laboratory.[6] In addition to rupture time and stress, the strain was measured periodically throughout the test (see Figure 11). Both primary and secondary stages are observed; the third stage is very short.

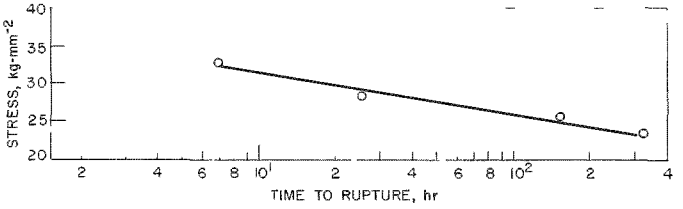

Figure 10. Tangential Stress vs. Rupture Life for Seamless 304 Stainless Steel Tubing in Argon at 550°C

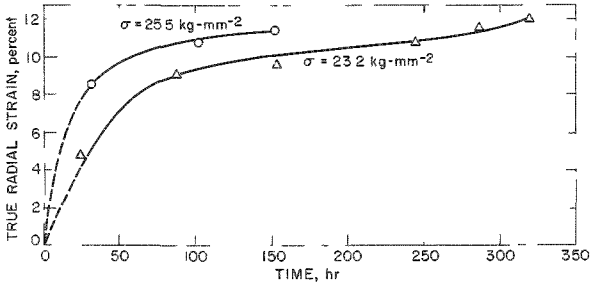

Figure 11. True Radial Strain vs. Time for Seamless 304 Stainless Steel Tubing in Argon at 550°C

Tests of Nb-1 w/o Zr alloy tubing at 500 and 600°C showed that creep occurred only within a very narrow range of stress between the yield stress and the ultimate (spontaneous rupture) stress. This is in agreement with similar behavior previously reported[7] for uniaxially tested rod specimens. The pressurizing system must be absolutely free of leaks to permit testing within this very narrow range of stress. Some results are presented in Table X. There is an increase of spontaneous rupture stress with longer pre-exposure time at temperature, suggesting a possible time-dependent specimen strengthening. This could be due to specimen contamination at 1×10^{-6} Torr testing environment or to the small amount of strain that occurred during the pre-exposure under stress. Samples of the tested specimens have been submitted for analysis.

[6] Manly, W. D., and Hobbs, J. H., "Experimental Gas Cooled Reactor," Nuclear Metallurgy, Vol. VIII, AIME, New York (1962) p. 63.

[7] ANL-6868, Metallurgy Division Annual Report for 1963, p. 132.

Table X. Tube-burst Data for Stress-relieved Nb-1 w/o Zr Alloy at 550 and 600°C

Pre-exposure Conditions			Stress for Spontaneous Rupture ($kg\text{-}mm^{-2}$)
Time (hr)	Stress ($kg\text{-}mm^{-2}$)	Strain (%)	
	550°C		
	None		33.6
336	29.6	0.44	34.2
493	32.6	0.93	35.8
	600°C		
	None		32.8
>345	33.3	>1.25	Test still in progress

Tubular specimens of V-20 w/o Ti alloy are being prepared for testing in vacuum with and without pre-exposure to flowing sodium.

(iv) Young's Modulus of TV-20. Additional values (see Progress Report for June 1964, ANL-6912, p. 24) have been determined for the static Young's modulus of TV-20 in the temperature range from 500 to 650°C (see Figure 12).

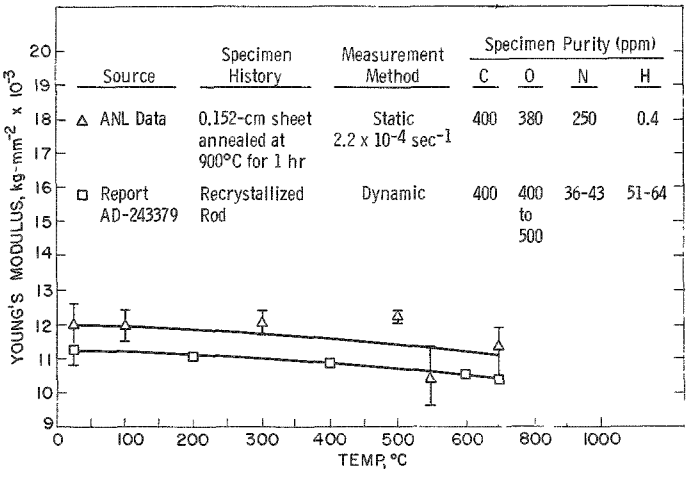

Figure 12
Young's Modulus vs. Temperature for TV-20

(v) Corrosion by Sodium. Analysis of the corrosion product from TV-20 tensile samples exposed to flowing (15 cm/sec) sodium for 7 days at 650°C has continued. The presence of $VO_{0.9}$ in the corrosion product was determined by X-ray diffraction. Wet chemical techniques

indicated the presence of 14 w/o V and 28 w/o Ti. Spectrochemical analysis showed the presence of 10 w/o Na in the corrosion product. There is evidence that this sodium was not in the corrosion product as free Na_2O or NaOH, but the exact nature of the sodium component (e.g., a complex sodium titanate) has not been determined.

Development of a suitable sampling-analytic technique for the determination of oxygen in sodium at low concentrations ($\lesssim$25 ppm) is satisfactory. Duplicate sodium samples taken from a liquid sodium bath at 140°C yielded results of 6.1 and 5.5 ppm oxygen. The equilibrium solubility of oxygen in sodium at 140°C has been reported as 7.5 to 8.0 ppm.[8]

A test chamber has been fitted with a small diaphragm pump that forces the sodium through a cold trap maintainable at any desired temperature for control of the oxygen content. An excess of sodium peroxide is added before testing. This insures an adequate amount of oxide in the cold trap to supply losses of oxygen due to sample corrosion during the test. The flow rate is such that a volume equal to that of the system passes through the cold trap in about one hour.

The first alloys tested were exposed one week (168 hr) to sodium at 650°C containing about 50 ppm oxygen (analysis: start 42 ppm; finish 50 ppm). This concentration is maintained with a cold-trap temperature of 250°C. The preliminary results are shown in Table XI.

Table XI. Corrosion of Vanadium-Titanium-based Alloys in 650°C Sodium Containing up to 50 ppm Oxygen

Alloy*	Loss in Thickness,** cm x 10^3
V-20 Ti	9.2
V-15 Ti-5 Cr (No. 1)	4.8
V-15 Ti-7.5 Cr (No. 2)	4.3
V-30 Ti-5 Cr (No. 5)	2.8
V-30 Ti-10 Cr (No. 6)	3.5

*Alloy compositions in weight percent. Samples tested were cold reduced about 50%.

**As measured with micrometer after removal of loose corrosion product.

[8]Salmon, O. N., and Cashman, T. J., KAPL-1653.

The samples were coated with a dark, nonadherent corrosion product. This was removed by brushing prior to the above thickness measurements. A dark adherent film was retained by the specimens. Chromium in amounts of about 5 to 8 w/o appears to be a beneficial addition, confirming earlier tests made with small arc-melted buttons under less carefully controlled oxygen conditions. However, no final conclusions should be drawn until the results of microscopic examination and microhardness traverses are available.

3. Zero-power Reactor Fuels

a. Zero-power Uranium-Plutonium-based Fuel Alloys. U-Pu metal alloys are favored as the fuel in critical experiments for future fast power breeder reactors. The selection of the U-20 w/o Pu-2.5 w/o Mo as the fuel alloy for the SEFOR fast critical experiments in ZPR-III was based on its excellent room-temperature air-corrosion resistance, high ignition temperature, good thermal expansion characteristics, high strength, good metallurgical stability, and reasonable fabricability. The results of the air-corrosion test of several U-Pu base alloys are summarized in Figure 13; in this figure "INT. CHILL CAST" denotes "intermediate-chill cast."

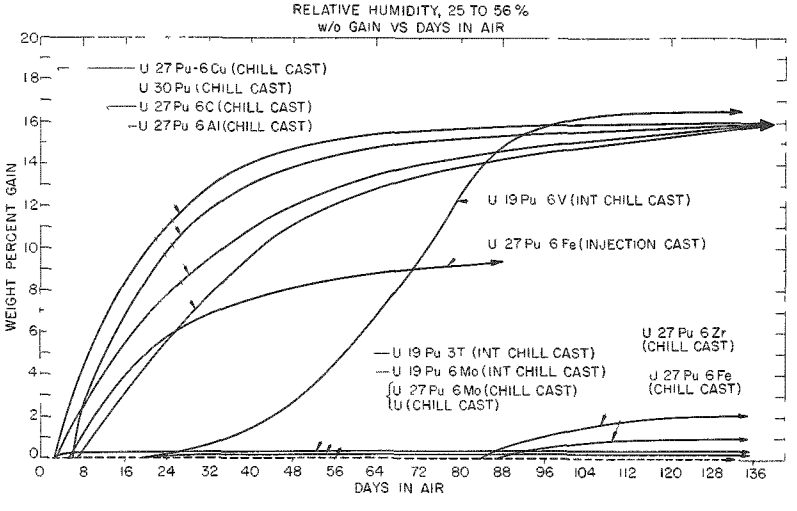

Figure 13. Room-temperature Air-corrosion Tests of U-Pu-X Alloys (Composition in a/o)

The specific heat for the U-20 w/o Pu-2.5 w/o Mo alloy reported in the Reactor Development Program Progress Report, July 1964, ANL-6923, p. 27, should be 0.037 rather than 0.37 cal g^{-1} $°C^{-1}$.

Two jacketed, 5.1 x 7.6-cm (2 x 3-in.) SEFOR fuel plates in storage for six months show no swelling or other evidence of fuel instability.

Air corrosion and metallographic studies indicated that titanium, an element favorable from physics considerations, may be a satisfactory alloying addition. The air-corrosion test of a U-20 w/o Pu-1.3 w/o (6 a/o) Ti (nominal composition) alloy has continued. Chemical analysis showed this specimen to contain only 0.57 w/o Ti (2.77 a/o). The specimen began to powder, but appeared relatively sound after 2 mo of air-corrosion testing. After 7 mo the specimen was approximately 30% disintegrated to powder, and the remainder had broken into several pieces.

Air-corrosion tests have been started on castings of U-26.3 w/o Pu-1.3 w/o Ti (U-25 a/o Pu-6 a/o Ti) and U-27.7 w/o Pu-2.7 w/o Ti (U-25 a/o Pu-12 a/o Ti). Both have shown no weight gain after two weeks.

Although zero-power fuels are normally used at room temperature, their expansion characteristics at higher temperatures should be known in case of a reactor excursion. The dilatometric data in Table XII were obtained on the as-cast alloys.

Table XII. Expansion Characteristics of U-Pu-Ti ZPR Alloys

Alloy Compositions (a/o) (w/o)	25 Pu-6 Ti 26.3 Pu-1.3 Ti	25 Pu-12 Ti 27.7 Pu-2.7 Ti
Expansion Coefficient, x 10^6/°C 25°C to Transformation	22.2	23.3
Transformation Range, °C	580-673	568-732
Expansion, $\Delta\ell$	0.52%	0.94%
Expansion Coefficient, x 10^6/°C Transformation to 860°C	15.3	25.3

E. General Fast Reactor Fuel Reprocessing Development

1. Skull Reclamation Process

The skull reclamation process (see Progress Report for December 1964, ANL-6997, p. 8) is being developed as an auxiliary process to recover and purify uranium from the skull remaining in the crucible after melt refining. Four runs with oxidized melt refining skulls have been completed in a series of six replication experiments which should complete the pilot-plant demonstrations of this process on a 1.5-kg scale.

Special attention is being given to achieving high uranium recovery. In the past, there has been excessive entrainment of a uranium-zinc intermetallic compound in the supernatant metal solution during its transfer to

waste. The intermetallic precipitation step of one run was performed a total of six times with several operational variations in an attempt to study the variables affecting uranium entrainment. Final results for this run are not yet available. However, preliminary results obtained in this and other recent runs indicate that uranium entrainment has been reduced to a low value (~1%). The major operating change which has decreased entrainment is the reduction of backflushing of gas through the transfer line prior to transfer of the supernatant metallic solution. While the temperature is being lowered to 625°C and the major portion of the intermetallic is precipitating, backflushing is done to keep the transfer line free of precipitate. Since the transfer line extends through the supernatant metal phase and into the intermetallic bed, backflushing tends to keep some of the intermetallic precipitate in suspension.

2. Halide Slagging Studies

The attractiveness of fast breeder reactors depends, in good measure, on the ability to separate bred plutonium readily from the fertile uranium blanket. One possible method to accomplish this is to oxidize the plutonium with uranium trichloride. Since the amount of UCl_3 required is small, $CaCl_2$ is being used as a diluent to assist in separation of the equilibrated phases. The chemical reaction on which this procedure is based is

$$UCl_3(CaCl_2) + Pu(U) \rightleftarrows PuCl_3(CaCl_2) + U.$$

A series of experiments has been instituted to determine the chemical equilibrium in this reaction at 1150 and 1250°C.

Four scoping experiments, including one blank run in which no uranium trichloride was present, have been performed. In these experiments, the salt and metal phases were contacted at 1200°C for periods of 15 to 90 min, after which the salt phase and metal phase were separately analyzed for plutonium. The mole ratios of UCl_3:Pu in the starting materials were approximately one (0.93 to 1.17). Preliminary results indicate that between 15 and 30 min were required to reach equilibrium. The plutonium vaporized during the 30-min experiment was approximately 1%.

For one experiment for which complete data are available, the equilibrium constant for the above reaction had a value of 85 to 119. A satisfactory single-stage extraction process for the recovery of plutonium from discharged blanket material would require a minimum equilibrium constant of about 75.

3. Decladding Studies for TV-20 Cladding

Metallic fuels for fast breeder reactor cores are expected to consist of uranium and plutonium alloyed either with fissium (Fs) or with refractory metals such as titanium or zirconium. The cladding is likely to be either TV-20 (vanadium-20 w/o titanium) or stainless steel. Mechanical decladding of high-burnup fuels may not be feasible because of bonding between the fuel and cladding. Chemical methods for separating fuel from cladding materials are therefore being investigated.

Final analyses have been received for the experiment (see Progress Report for January 1965, ANL-7003, p. 22) in which a U-20 w/o Pu-10 w/o Fs alloy clad in TV-20 was hydrided, dehydrided, and contacted by stirring for 10 hr with Cd-15 a/o Zn-15 a/o Mg and LiCl-KCl eutectic at 600°C. The analyses of filtered samples of the liquid metal phase showed 96% of the plutonium but only 55% of the uranium to be in solution. Impurities in the salt or in the glovebox atmosphere are the suspected cause for the failure of some of the uranium to appear in solution. Additional experiments are planned to improve the uranium recovery.

In another laboratory-scale experiment, uranium-fissium alloy clad with TV-20 was hydrided, dehydrided, and contacted with molten cadmium at 400°C. Examination of the solidified (~2-cm-dia) ingot revealed a thin (~0.2-cm) top layer of TV-20 fragments, a thicker (~0.5-cm) intermediate layer of cadmium metal, and a deep (~3-cm) bed of uranium-cadmium intermetallic compound at the bottom. This result suggests the possibility of separating TV-20 cladding fragments by flotation in liquid cadmium.

4. Processes for Advanced Reactor Fuels

The developmental program for advanced fuel processes is presently concentrated on studies of mass transfer rates between liquid metal and liquid salt phases at high temperatures. The objectives are to demonstrate the feasibility of continuous metal-salt extractions, to determine optimum operating conditions, and to obtain a clearer understanding of the extractive process.

Experiments were made to determine the rate of uranium transfer from a liquid Cd-3.5 w/o Mg alloy into a chloride salt (50 m/o $MgCl_2$, 30 m/o NaCl, 20 m/o KCl) at 550 to 600°C when the metal was passed through static salt in packed columns. The overall mass transfer coefficient based on the salt phase was found to be between 0.0036 and 0.0076 sec^{-1}. Somewhat higher values would be expected in steady-state countercurrent packed columns. The above values imply a height for one theoretical stage of 2 to 5 ft for a typical packed extraction column in

which plutonium[9] is separated from rare earths. Stage heights in the above range would be satisfactory. More accurate determinations of stage height will be made in future runs with packed columns.

In addition to various column-extraction tests being made, studies of the mixer-settler extraction process have begun. Runs are being made to determine the residence time and degree of agitation necessary to achieve good separation in a mixer-settler unit. In batch tests to study mixing parameters, the rate of cerium transfer from a liquid Cd-Zn-Mg alloy into a chloride salt in an agitated vessel was determined for mild, moderate, and vigorous agitation. With mild agitation (60 rpm), the mass transfer rate in an unbaffled vessel was very low and was limited by a large concentration gradient in the metal phase. With moderate agitation (flat paddle rotated at 350 rpm) in a baffled vessel, the two phases reached greater than 95% of equilibrium in 45 min. An experiment involving vigorous agitation (700 rpm) has also been completed, but results are not available.

---

[9]Plutonium and uranium are assumed to have the same mass transfer coefficients.

II. GENERAL REACTOR TECHNOLOGY

A. Experimental Reactor and Nuclear Physics

1. The Am-α-Li Neutron Spectrum

The Am-α-Li neutron spectrum is well-suited for use in studying the 4π recoil techniques.[10] The neutron spectrum is expected to be similar to that produced by the Po-α-Li reaction; americium alphas are about 180 keV more energetic than are those for polonium. The mean neutron energy is about 0.5 MeV.

The source consisted of 0.43 g of AmO_2 mixed with 5.0 g of natural lithium, encapsulated in stainless steel and placed in a double-walled stainless steel capsule. The total mass of source and container was 85 g. The total neutron emission was about 1.0×10^5 per sec.

Spectrum measurements were made with the use of two different recoil-proton probes. The first was 5.0 cm in diameter, had a wall thickness of 0.8 mm, and was filled to a pressure of $2\frac{1}{2}$ atm of CH_4, including N_2 for calibration at a pressure of 10 cm of Hg. Recoil-proton spectra between 75 and 1400 keV were recorded. A second probe, having a 2.5-cm diameter, a 7-cm effective length, and a wall thickness of 1.2 mm, was filled to a pressure of 3 atm of H_2 (10 cm of Hg of CH_4 for quenching and an equal amount of N_2 for calibration). Measurements were made in the energy interval between 20 and 110 keV. Both counters were shielded with lead during the experiment.

No corrections were made for a variation of ionization potential W with energy for the results from the methane counter. Existing data[11] indicate that W probably does vary somewhat over the interval from 100 keV to 1 MeV for CH_4, but is not adequate to permit its use for making corrections. The range of 1-MeV protons in the 5-cm-diameter methane counter is 1.0 cm, and a significant correction for distortion of the measured recoil-proton spectrum by wall-and-end effects above 1 MeV is required.

The neutron spectrum derived from this experiment (resolution is approximately 20%) is shown in Figure 14, together with the earlier experimental results found by Barton[12] using a diffusion cloud chamber and the

---

[10] Bennett, E. F., A Study of the 1/E Slowing-down Neutron Spectrum Using 4π Recoil Proportional Counters, ANL-6897 (Sept 1964).

[11] Ferguson, A. T. G., Gas Recoil Counter, Fast Neutron Physics, (Interscience Publishers, Inc., New York, 1960, Marion, J. B., and Fowlers, J. L., Eds.).

[12] Barton, D. M., Measurement of the Neutron Spectrum from a Po-Li^7 Neutron Source, LA-1609 (July 1953).

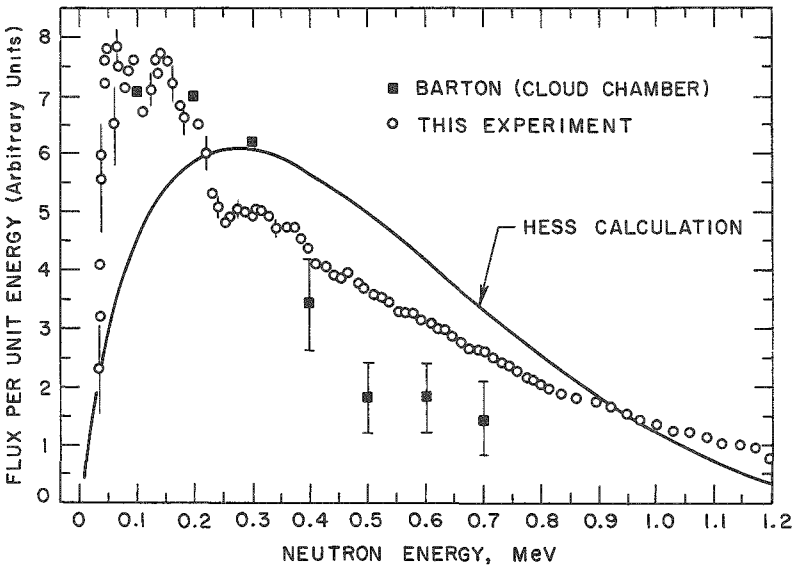

Figure 14

Neutron Spectrum from the Am-α-Li Reaction

calculated results of Hess.[13] The experimental data are in rough agreement but differ from the theoretical prediction. Reasons for this discrepancy have been offered by Hess. Since americium oxide does not alloy with lithium, it must therefore be mechanically mixed. If the diameter of AmO_2 particles is comparable with the alpha-particle range, then fewer energetic alphas will escape to bombard the lithium. The calculated neutron spectrum was made under the assumption of uniform mixing of alpha emitter and lithium material. In addition to the mixing problem, degradation of neutron energy also occurs by elastic scattering with lithium in the source and to a much lesser extent by inelastic scattering with the structural environment and lead shielding around the counter.

2. High Conversion Critical Experiment

The High Conversion Critical Experiment work has been completed and results are now being analyzed. In the course of analysis the cadmium ratios have been obtained for several foil materials (indium, copper, gold, and manganese). These cadmium ratios were found to be linear functions of the core moderating ratio over a wide range of core-loading densities. This linear relationship (see Figure 15) was used as a basis for organizing the available cadmium ratio measurements in the Hi-C cores. Similar linear plots have been obtained for U^{235} and U^{238} capture ratios.

The linearity of such curves is consistent with the following two-group considerations. Using the superscripts sub and epi to indicate the subcadmium and epicadmium groups, and the subscript x to indicate the foil material, one can write:

$$\text{CdR} - 1 = \frac{\text{subcadmium activation}}{\text{epicadmium activation}} = \frac{\sigma_{ax}^{sub}\,\phi_{x}^{sub}}{\sigma_{ax}^{epi}\,\phi_{x}^{epi}}, \qquad (1)$$

[13] Hess, W. N., Neutrons from (α,n) Sources, Ann. Phys. 2, 115 (1959).

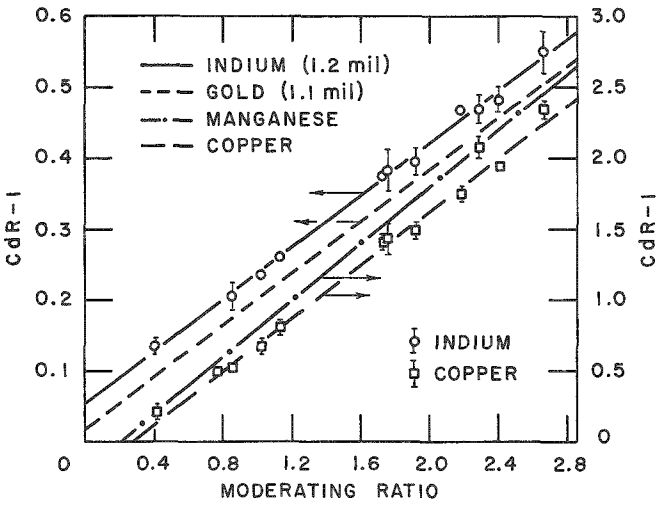

Figure 15

Cadmium Ratio as Function of Core Moderating Ratio. Curves are least-squares linear fits to experimental data.

where the absorption cross sections σ_a^{sub} and σ_a^{epi} are averaged over the subcadmium and epicadmium spectra respectively, and the flux ϕ_x is averaged over the foil position.

For internal lattice positions, neglecting leakage, a thermal-neutron-balance equation

$$\sum_i n_i \sigma_{ai}^{sub} \phi_i^{sub} = c \sum_i n_i \xi_i \sigma_{si}^{epi} \phi_i^{epi} \qquad (2)$$

can be written. Here n_i is the average number of atoms of core component i per unit cell volume, and c is an (approximate) constant of proportionality. Multiplying Eq. (1) by Eq. (2), rearranging, and considering that in the cores investigated the right-hand side of Eq. (2) was dominated by the hydrogen, with a small contribution from the oxygen, one obtains

$$CdR - 1 = c \frac{\sigma_{ax}^{sub}}{\sigma_{ax}^{epi}} \frac{\left(n\xi\ \sigma_s^{epi}\right)_H \left(\phi_H^{epi}/\phi_x^{epi}\right) + \left(n\xi\ \sigma_s^{epi}\right)_O \left(\phi_O/\phi_x^{epi}\right) + \ldots}{\left(n\ \sigma_a^{sub}\right)_f \left(\phi_f^{sub}/\phi_x^{sub}\right) + \left(n\ \sigma_a^{sub}\right)_H \left(\phi_H^{sub}/\phi_x^{sub}\right) + \ldots} . \qquad (3)$$

The foils were located between fuel pellets, so that $(\phi_f^{sub}/\phi_x^{sub}) \approx 1$. It happens that the other flux ratios in Eq. (3) can also be set equal to unity without introducing much error, since the epicadmium flux is typically quite flat and since the denominator of Eq. (3) is dominated by the first term. Now one can write

$$CdR - 1 \approx c \frac{\sigma_{ax}^{sub}}{\sigma_{ax}^{epi}} \frac{\left(n\xi\ \sigma_s^{epi}\right)_H + \left(n\xi\ \sigma_s^{epi}\right)_O + \ldots}{\left(n\ \sigma_a^{sub}\right)_f + \left(n\ \sigma_a^{sub}\right)_H + \ldots} \approx \text{const (MR)}, \qquad (4)$$

where MR is the moderating ratio.

Thus it is predicted that the cadmium ratio in the fuel should be approximately a linear function of the moderating ratio even if the latter is calculated on the basis of a homogenized core.

The fact that the extrapolated curves of Figure 15 do not pass closer to the origin is perhaps due to spectral changes from core to core, since the "const" of Eq. (4) contains effective foil cross sections which are somewhat dependent upon the spectral shape.

The linear plots in Figure 15 come from cores with two different cladding materials (aluminum and stainless steel, two fuel diameters (0.87 cm and 0.935 cm), and two fuel compositions (3 and 5 w/o enriched UO_2).

These results provide a simple test for calculations on neutron spectra and material reaction rates.

B. Theoretical Reactor Physics

1. Resonance Interference

A program has been written for the CDC-3600 to compute resonance absorption by a rod in a two-region cell. Since the program is not based on the narrow-resonance approximation in the moderator, it is capable of computing absorption by wide resonances or by overlapping resonances more accurately than methods based on that assumption.

An energy range of interest is divided into many groups, whose equal lethargy width is much less than the maximum lethargy gain per collision with uranium. The source distribution for a group is taken to have the form

$$S_i = \sum_{n=0}^{2} S_{in}\left(\frac{r}{a}\right)^{2n},$$

where a is the radius of the rod, i = 0 for the rod, and i = 1 for the moderator. The collision rate in the rod is given by

$$C_{rod} = S_s(1 - p_s) + \sum_{n=0}^{2} (1 - p_n)S_{on}, \qquad (1)$$

where S_s, the rate at which neutrons impinge upon the surface of the rod, is

$$S_s = \sum_{n=0}^{2} \left\{ P_{an} S_{1n} + \frac{T_{ba} \left[p_n T_{ab} S_{on} + (P_{bn} + P_{an} p_s T_{ab}) S_{1n} \right]}{1 - T_{bb} - T_{ba} T_{ab} p_s} \right\}, \qquad (2)$$

with

P_{xn} ≡ first flight escape probability through moderator surface at x for neutrons from S_{1n};

T_{xy} ≡ probability that isotropic flux incident upon moderator at x escape through the surface at y;

p_n, p_s ≡ first flight escape probabilities from the rod for neutrons from S_{on} and S_s, respectively.

Cady's moment method[14] is used to obtain the escape probabilities from the rod and the flux in the rod in the form

$$\phi(r) = \sum_{n=0}^{2} \phi_n \left(\frac{r}{a}\right)^{2n}. \qquad (3)$$

The flux in the moderator, in the form

$$\psi(r) = \sum_{n=0}^{2} \psi_n \left(\frac{r}{a}\right)^{2n}, \qquad (4)$$

is then obtained from the conditions of neutron conservation, equality of the fluxes at the interface, and vanishing of the derivative of the flux at the edge of the cell. These fluxes then contribute to the source for lower groups. Calculations of p for the water-moderated cells considered by Rothenstein[15] were in excellent agreement with his Monte Carlo results.

2. Solution of Transcendental Equations by Series Reversion

One of the more common computing tasks is the solution of non-linear algebraic and transcendental equations of the form

$$F(Y) = G(X). \qquad (1)$$

For a single value of X, such equations may ordinarily be solved by iteration, provided an adequate initial approximation to the root is available. In

[14] Cady, K. B., and Clark, M., Neutron Transport in Cylindrical Rods, Nucl. Sci. Eng. 18, 491-507 (1964).

[15] Rothenstein, W., Some Monte Carlo and Analytic Results for Resonance Capture in Lattices, Nucl. Sci. Eng. 8, 122-127 (1960).

many cases, however, an analytical approximation to the root is desirable, either to furnish starting values for the iteration, or for direct application when only limited accuracy is required.

Let Eq. (1) have a known root, Y_0, at $X = X_0$. Let $F(Y)$ be analytic in the neighborhood of Y_0, and let $G(X)$ be analytic in the neighborhood of X_0. Further, suppose that $F'(Y_0) = F'_0 = 0$. Then the variable transformations $y = Y - Y_0$ and $x = X - X_0$ allow us to write Eq. (1) in the form

$$f(y) = \frac{F(y+Y_0) - F(Y_0)}{F'_0} = g(x) = \frac{G(x+X_0) - G(X_0)}{F'_0}, \tag{2}$$

where $f(y)$ and $g(x)$ have the convergent power series representations

$$f(y) = \sum_{j=1}^{\infty} a_j y^j, \qquad g(x) = \sum_{i=1}^{\infty} b_i x^i, \tag{3}$$

with $a_1 = 1$.

We have developed an algorithm for finding the coefficients in the power series for $y(x)$, where y is the root of Eq. (2), from the coefficients in the power series for $f(y)$ and $g(x)$. For $g(x) = x$, the algorithm reduces to the familiar one for reversion of power series.

For $j = 1, 2 \ldots$, let y be a root of Eq. (2) and let

$$y^j = \sum_{i=j}^{\infty} c_{i,j}\, x^i, \tag{4}$$

so that the desired coefficients are the $c_{i,1}$. The existence and continuity of y are assured in a neighborhood of 0 by the implicit function theorem.

Since $y^{j+1} = yy^j$, we may take the product

$$y^{j+1} = \sum_{i=1}^{\infty} c_{i,1}\, x^i \sum_{i=j}^{\infty} c_{i,j}\, x^i = \sum_{i=j+1}^{\infty} \sum_{k=1}^{i-j} c_{k,1}\, c_{i-k,j}\, x^i, \tag{5}$$

and the $c_{i,j}$ obey the recurrence for $i > j \geq 1$,

$$c_{i,j+1} = \sum_{k=1}^{i-j} c_{k,1}\, c_{i-k,j}. \tag{6}$$

Substituting Eq. (4) into (3) and rearranging, we obtain

$$\sum_{j=1}^{\infty} a_j y^i = \sum_{j=1}^{\infty} \sum_{i=j}^{\infty} a_j c_{i,j} x^i = \sum_{i=1}^{\infty} \sum_{j=1}^{i} a_j c_{i,j} x^i = \sum_{i=1}^{\infty} b_i x^i; \tag{7}$$

accordingly,

$$c_{i,1} = b_i - \sum_{j=2}^{i} a_j c_{i,j}. \tag{8}$$

Thus the algorithm for computing the $c_{i,j}$ is as follows: Set $c_{1,2} = b_1$. For i = 2, 3, ..., compute $c_{i,j+1}$ for j = i - 1, i - 2, ..., 1 by use of Eq. (6); then compute $c_{i,1}$ by use of Eq. (8). The $c_{i,1}$ are the desired coefficients.

The resulting power series for y(x) can be used in a variety of ways. In addition to direct application, the series may be transformed to a series in Chebyshev polynomials, which may be truncated to give a nearly minimax approximation over a specified range. Other possibilities include conversion to Padé approximants, and application of the various devices for accelerating convergence.

3. Multigroup Neutron Fluxes in a Subcritical Multiplying Medium with a Constant External Source

The problem of solving for the neutron flux in a subcritical, finite, multiplying medium with a constant external neutron source often arises in reactor physics. The methods, outlined below, for obtaining the neutron fluxes are applications of the technique of following neutron reaction rates through many successive generations. Multigroup diffusion theory is used to provide the setting for this discussion, but it is not an essential feature of the methods.

The N-group equations for the neutron flux, $(\phi_j) \sum_{j=1}^{N}$, is written in the symbolic form

$$0 = L_j \phi_j + \sum_{k=1}^{N} \Sigma_{\text{source}}(k \to j)\phi_k + S_j^e, \qquad 1 \leq j \leq N. \tag{1}$$

Here $L_j \phi_j$ is the loss rate of group-j neutrons due to net leakage and to the various removal processes; $\Sigma_{\text{source}}(k \to j)\phi_k$ is the rate of injection of neutrons into group j, from events of scattering, fission, and (n,2n) in group k; and S_j^e is the external source rate for group j. All functions are assumed to be functions of the position vector, $\underline{r}$.

Equation (1) may be solved, by the method of successive generations, by setting $\phi_j = \sum_{m=0}^{\infty} \phi_{m,j}$, and solving Eq. (2) as follows:

$$0 = L_j \psi_{m,j} + \sum_{k=1}^{N} \Sigma^*_{source}(k \to j) \psi_{m,k} + S_{m,j}; \qquad 1 \leq j \leq N, \tag{2}$$

where

$$\Sigma^*_{source}(k \to j) \equiv \Sigma_{source}(k \to j) - \beta_j (\nu \Sigma_f)_k$$

and

$$S_{m,j} \equiv \begin{cases} S^e_j, & m = 0 \\ \beta_j \sum_{k=1}^{N} (\nu \Sigma_f)_k \psi_{(m-1),k}; & m \geq 1. \end{cases}$$

Thus, for $m = 0$, the source is the external source. For $m \geq 1$, the source for the m^{th} neutron generation is the unrenormalized fission neutron production rate resulting from events in the $(m-1)^{th}$ generation. This corresponds to a sequence of "one-shot" problems of the type which the REX program can solve for one-dimensional problems where the source and the medium have suitable spatial symmetry.

The advantage of this method is that the flux contributions from the various neutron generations are displayed. However, to obtain the total flux $\phi_j(\underline{r})$, in group j, it is necessary to sum the components $\psi_{m,j}$. If this intermediate information is not desired, an alternative procedure is to solve the sequence of problems:

$$0 = L_j \tilde{\psi}_{m,j} + \sum_{k=1}^{N} \Sigma^*_{source}(k \to j) \tilde{\psi}_{m,k} + \tilde{S}_{m,j}; \qquad 1 \leq j \leq N, \tag{3}$$

where

$$\tilde{S}_{m,j} \equiv \begin{cases} S^e_j; & m = 0 \\ S^e_j + \beta_j \sum_{k=1}^{N} (\nu \Sigma_f)_k \tilde{\psi}_{(m-1),k}; & m \geq 1. \end{cases}$$

Then

$$\tilde{\psi}_{m,j} = \sum_{n=0}^{m} \psi_{n,j},$$

and

$$\phi_j = \lim_{m\to\infty} \tilde{\psi}_{m,j}.$$

The functions $\psi_{m,j}$ converge rapidly, in shape, to the asymptotic distribution in a fictitious critical medium where all $(\nu\Sigma_f)_k$'s have been multiplied by $1/k_{eff}$. To estimate the remainder,

$$\sum_{m=M}^{\infty} \psi_{m,j},$$

after M steps, assume that the process has been carried to the point where, for $m \geq M$, $k_{eff_m} \approx k_{eff}$, and $\psi_{m,j} \approx k_{eff}\, \psi_{(m-1),j}$.

Then

$$\sum_{m=M}^{\infty} \psi_{m,j} \approx \frac{k_{eff}}{1 - k_{eff}}\, \psi_{(M-1),j}.$$

Here, k_{eff_m} is defined as the ratio

$$k_{eff_m} \equiv \frac{\int_{medium} \sum_{k=1}^{N} (\nu\Sigma_f)_k\, \psi_{m,k}\, dV}{\int_{medium} \sum_{k=1}^{N} (\nu\Sigma_f)_k\, \psi_{(m-1),k}\, dV}.$$

In computer programs which might be based upon Eq. (3), it would be desirable to provide an option of flux convergence, where the convergence of fluxes in certain energy groups and in certain regions is specified. An additional convergence criterion should be stated, namely, on k_{eff_m}, for example, a Cauchy condition on k_{eff_m} which would be tested by computing

$$\left| k_{eff_{(m-p)}} - k_{eff_{(m-p^*)}} \right|$$

for a certain number of values p and p*, say $0 \leq p \leq p_0$, and $0 \leq p \leq p_0$; or, perhaps, first k_{eff} could be calculated, with a convergence criterion that

$$\left| k_{eff_{(m-p)}} - k_{eff} \right| < \epsilon \quad \text{for } 0 \leq p \leq p_0.$$

C. High-temperature Materials

1. Ceramics

a. Properties of (Th-U) Phosphides. Study of the properties of UP has continued. Measurements of electrical resistivity, made on samples sintered or heat treated in the temperature range from 1600 to 2200°C, showed no clear-cut relationship between room-temperature resistivity and heat-treatment temperature, despite the small differences in stoichiometry arising from heating at different temperatures and the presence of metallic uranium in samples fired at 2000°C or higher.

The curve of thermal expansion of UP over the range from 20 to 980°C was continuous and showed a slight increase in expansivity with rising temperature. The thermal expansion value to 980°C was 8.6×10^{-6} cm/cm-°C, somewhat lower than those for UO_2 or US.

Final investigations were made of the system UP-UO_2. The phase diagram of the system was comparatively simple, with no intermediate compounds and no solubility between the phases. A eutectic occurred at the composition UP-58 m/o UO_2 and a temperature of 2390 ± 30°C. The melting temperatures in helium were 2535°C and 2720°C for UP and UO_2, respectively. It is likely that at their melting temperatures both compounds were hypostoichiometric. Moreover, small amounts of metallic uranium most probably formed above 2200°C, through decomposition of UP and possibly of UO_2. Accelerated vaporization of intermediate compositions in the system was thought to be partly due to the high-temperature reaction $UP + UO_2 \rightarrow 2UO\uparrow + P\uparrow$. The occurrence of metallic uranium at UP-UO_2 boundaries in material fired at 2000°C suggests that another high-temperature reaction between the two compounds was responsible for its formation. However, this cannot be stated unequivocally, since photomicrographs of pure UO_2 fired at 2000°C in vacuum also showed the presence of substantial amounts of uranium in grain boundaries. Moreover, it is possible that in both cases the metal precipitated out during sample cooling.

b. Mechanical Properties of UO_2. Results obtained over the previous four months and requiring further explanation to elucidate the mechanisms of deformation have been rechecked.

Two batches of specimens were examined at 1500°C, at medium and high strain, with high density, achieved by eliminating the use of Carbowax binder in pressing. (The green strength of such compacts is low, and 5 to 10% of the specimens are lost through handling damage or through premature cracking due to thermal shock in sintering. The method does, however, ensure high density, up to 10.64 g/cc.) The previous trend of results at 1500°C was confirmed, i.e., that some porosity assists

relaxation of stress and confers ductility on the specimens, so that a higher maximum stress is possible, but higher strain rate always results in a high maximum stress in ductile specimens. Crack propagation velocity must therefore be fairly slow at 1500°C, and, above a critical strain rate, lags behind the rate of increase of stress. The total deformation decreases with higher strain rate, however, since less time is available for relaxation at a number of suitable sites.

Similar confirmatory tests were made at 1200°C and room temperature. Previous specimens tested at 1200°C were of early batches of materials, with lower density. The room-temperature specimens had all been tested in air on previous occasions, as for all previously published work, so far as can be ascertained. The new batches, tested in vacuum, showed higher maximum stress, sometimes by a factor of 2. The suggested explanation for this change is the presence of moisture in the air, which accelerates crack propagation as in stress-corrosion phenomena.

Tests were carried out at 1750°C and 1500°C for specimens from which the skin had been ground away to a depth of 1.52 mm on the tensile face. The higher-density layer on the surface has always been presumed to resist the nucleation of cracking to a greater degree than the more porous interior, but results showed that the modulus of rupture was higher in ground specimens. This could be due to greater freedom from minor flaws or imperfections in the ground surface, or to the increased number of nucleation sites in the more porous surface exposed, leading to improved stress relaxation, or both.

Tests are now in progress at 1500°C with variations in atmosphere. Helium gas at 1 mm Hg pressure increased the plasticity of UO_2 at this temperature, reducing the yield point and maximum stress. This may result from moisture condensing after expansion from the gas cylinder, and in further tests use will be made of a drying tower to check this point.

These results, summarized in Table XIII, include the previous results for room-temperature tests in air.

Table XIII. Mechanical Test Data for UO_2

Number of Samples in Batch	Density (g/cc)		Maximum Stress (kg/cm^2)		Mean Strain Rate (mm/sec x 10^4)	Mean Total Strain (mm)	Temp (°C)	Atmosphere
	Mean	Standard Deviation	Mean	Standard Deviation				
5	10.58	0.009	843	128.0			25	Air
5	10.44	0.07	598	37.2			25	Air
5	10.64	0.001	1511	91.4	1.54	0.13	25	Vacuum
5	10.59	0.005	1480	91.4	4.24	0.10	25	Vacuum
5	10.61	0.005	1317	111.6	17.27	0.20	1250	Vacuum
4	10.58	0.01	1110	76.0	0.97	0.36	1500	Vacuum
4	10.60	0.007	1213	109.5	2.11	0.34	1500	Vacuum
3	10.62 ground to 10.60	0.005	1228	72.2	10.4	0.43	1500	Vacuum
2	10.50 ground to 10.48	0.05	1278	94.9	13.21	1.98	1750	Vacuum
2	10.6	0.005	867	15.0	13.05	0.40	1500	Helium

c. Thermal Stability. Current studies of thermal stability are concerned with determination of evaporation rates of materials and the evaluation of associated reactions.

(i) MgO. Determinations of evaporation rate of MgO in vacuum, for purposes of calibration, have been limited to 2330°K because of the excessive reaction of the evaporating species with tooling materials at higher temperatures. Some further studies will be made with MgO in helium.

The evaporation rate curve determined for MgO in vacuum is shown in Figure 16 for the temperature range from 1864 to 2333°K. The minimum and maximum rates in this range were 1.29×10^{-7} and 2.77×10^{-4} gm/cm^2 sec, respectively.

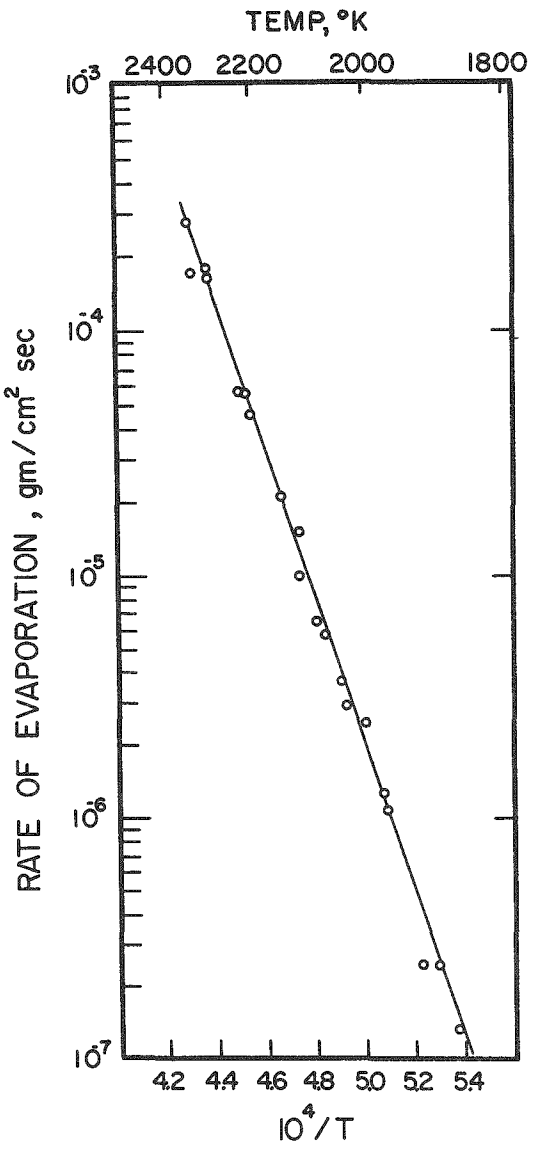

Figure 16. Evaporation Rate Data for MgO (System Pressure 1.0×10^{-5} to 1.2×10^{-6} Torr).

(ii) UO_2. Some determinations of evaporation rates of UO_2 in vacuum have been made in the temperature range from 1859 to 2418°K. Confirmation tests are in progress before establishing the evaporation curve in this temperature range.

(iii) Plutonium Ceramics. The evaporation behavior and oxidation resistance of plutonium ceramics will be studied. A high-temperature vacuum microbalance apparatus is being constructed for evaporation studies. Another apparatus is being set up for oxidation experiments involving gas-chromatographic analysis. In order to evaluate the performance of the oxidation apparatus and supplement existing data, preliminary experiments have been started on the oxidation behavior of uranium monosulfide.

d. Anelasticity of Some Uranium Compounds. Several attempts were made to oxidize specimens of uranium dioxide. The sample was placed in a reaction vessel and, after evacuating, oxygen was introduced. The temperature was raised in 30 min to 650°C, at which time a reaction started. After 3 min, the vessel was evacuated and quenched. The

specimens showed formation of U_3O_8 at the surface, attributed to the fact that the absorption of oxygen took place at a faster rate than diffusion into the body. The same results were obtained when trying to oxidize the sample in air at 300°C.

Next, a bar of uranium dioxide and a certain amount of U_3O_8 will be sealed in vacuum in a small container and heated at about 1000°C for 7 days. It is expected that by this technique, the oxygen evolved from the U_3O_8 powder will oxidize the sample; at the same time the formation of U_3O_8 in the specimen will be prevented, because the oxide will be unstable under this condition.

Samples for the study of the effect of grain size on Young's modulus and internal friction are being prepared. The first batch produced samples with a large number of pores. They were produced by the improper burnout of the binder. This defect was not present in subsequent batches, in which the binder was properly eliminated.

An existing furnace is being adapted for the high-temperature studies.

e. Uranium-mixed Anion Systems. Previously it was reported that UC dissolves in UP up to about 4 w/o at 1800°C in vacuum and that the solubility of UP in UC is negligible. The unit cell size of UP was 5.586 Å and of UP-4 w/o UC, 5.560 Å.

Some specimens used for the determinations above were further equilibrated by holding for 6 hr at 1800°C. After crushing to $<37\ \mu$ particle size, the resulting powders were pressed. These specimens were equilibrated for 4 hr at 1800°C. Unit cell sizes were determined from the X-ray diffraction patterns. The cell size of the UC was unchanged; however, the cell size for the UP(C) solid solution had increased. This increase was just opposite to what would be expected if equilibrium had not been attained in the initial equilibration. Consequently, it is thought that the presence of oxygen, 0.15% in the UP and 0.40% in the UC, caused the change, possibly by preferentially reacting with the dissolved UC. The fact that the equilibrated specimens were porous would allow this type of reaction to proceed.

2. Thorium-based Fuels

a. Th-U-Pu Irradiation Pins. Irradiation pins of two Th-U-Pu alloys, nominally Th-10 w/o U-10 w/o Pu (80-10-10 alloy) and Th-20 w/o U-10 w/o Pu (70-20-10 alloy), were prepared (see Progress Report for November 1964, ANL-6977, pp. 55-56). The alloys were selected from an isothermal section of the ternary phase diagram at 900°C because they contain no liquid phase at this temperature. They were fabricated from commercial materials into irradiation pins of 3.66 mm diameter (0.144 in.), heat treated

for 24 hours at 850°C and water quenched or, alternately, were given the same heat treatment, but were subsequently reheated for one hour at 700°C and furnace cooled.

The structures produced by the fabrication process and the heat treatments showed spherical or oblong α-uranium particles in a thorium matrix. The plutonium used in making these alloys contained:

0.00%	Pu^{238}
94.96	Pu^{239}
4.56	Pu^{240}
0.48	Pu^{241}
0.00	Pu^{242}

The uranium was 93.18% enriched. In two of the 70-20-10 alloys, normal uranium was added to produce an enrichment of 50% and create comparable enrichments for both the 80-10-10 and the 70-20-10 alloys.

The results of density determinations are listed in Table XIV. The heat treatment does not appear to affect the density.

Table XIV. Heat Treatments and Densities of Selected Irradiation Pins

No.	Alloy Th-U-Pu (w/o)	Uranium Enrichment (%)	Heat Treatment*	Density (g/cm^3)
B880-2	80-10-10	93.18	A	12.33
B880-1	"	93.18	B	12.32
B881-1	70-20-10	50	A	12.83
B882-1	"	50	B	12.88
B867-1	70-20-10	93.18	A	12.80
B867-2	"	93.18	B	12.81

*Heat treatments:

A: 24 hr at 850°C and water quenched.
B: 24 hr at 850°C and water quenched; subsequently reheated to 700°C, held for one hour, and furnace cooled.

A cast specimen heated to a temperature within 100 to 150°C of the solidus temperature in a vertical pushrod dilatometer begins to creep under the stresses produced by its own weight and the pushrod. Upon heating and cooling, a hysteresis-type loop[16] is recorded that becomes smaller and smaller in area as the cycle is repeated. The hysteresis eventually becomes negligibly small after 8 to 10 cycles. Prior heat treatment of the specimen at the maximum temperature of the cycle practically eliminates

[16]Actually, the initial loops are open at the bottom, because of creep, and therefore are not true closed hysteresis loops.

the hysteresis. Raising the temperature beyond the previous maximum makes it reappear. One possible explanation is that two superimposed phenomena are effective, one being homogenization of the original cast structure through replacement of a nonequilibrium low-melting phase by the equilibrium structure, the other one being progression of the first stage of creep rapidly enough to be observed by conventional dilatometry.

The coefficient of thermal expansion of the 80-10-10 alloy over the temperature range from 25 to 600°C varied with temperature from 12.2 to 13.2 x 10^{-6}/°C for stabilized alloys (alloys that showed no significant hysteresis).

The 70-20-10 alloy was stabilized by a 24-hr anneal at 850°C before making the dilatometric measurements. The linear coefficient of expansion for the temperature range from 25 to 587°C was found to be 13.1 x 10^{-6}/°C. The coefficient of expansion is smaller for lower temperature ranges.

b. Postirradiation Examination of Thorium-based Specimens. Postirradiation examinations of six thorium-based specimens irradiated in the CP-5 reactor are being conducted. These fuel specimens are 50 mm in length and 3.66 mm in diameter. All specimens were jacketed in Nb-1 w/o Zr tubing. The fuel alloys are Th-35 w/o Pu, Th-20 w/o U-20 w/o Pu, and Th-20 w/o U. The jackets had a wall thickness of 0.38 mm and an inside diameter of either 3.96 or 6.52 mm. The pins were NaK bonded to the jacket, but otherwise unrestrained. These fuel rods were irradiated to burnups ranging from a calculated 2.9 to 5.5 a/o heavy metal burnup and at maximum fuel temperatures of 780°C.

Surveillance of the condition of the specimens in the capsule was maintained by periodic examinations through neutron radiography. The capsule was disassembled when it was apparent that the fuel material in two specimens had deformed.

The hot-cell examination revealed that a Th-20 w/o U-20 w/o Pu specimen and a Th-35 w/o Pu specimen had ruptured the jacket. Both had been jacketed in 6.52-mm-ID tubing. The maximum irradiation temperatures were, respectively, 780°C and 720°C, at which temperatures a liquid phase would exist in the Th-U-Pu alloy and would also be highly probable in the Th-Pu alloy. From the radiographs it was possible to note that the fuel in these two specimens had divided into two separate pieces. Sections of the fuel completely filled the interior of the jacket. A small amount of fuel protruded from an opening in the jacket of the Th-35 w/o Pu-fueled specimen. The jacket of the specimen fueled with Th-20 w/o U-20 w/o Pu was badly deformed and cracked.

Another specimen, which was fueled with Th-35 w/o Pu and jacketed in 3.96-mm-ID tubing, had a longitudinal crack in the jacket. This specimen had been irradiated to 3.0 a/o burnup at a maximum fuel temperature of 570°C.

A specimen fueled with Th-20 w/o U and jacketed in 6.52-mm-ID tubing was intact, but the upper third of the fuel pin showed a marked diameter increase.

The jackets of the three intact specimens failed to show significant diameter changes. These specimens will be punctured for recovery and analysis of fission gas. All specimens will be sectioned for a detailed metallographic examination.

3. Corrosion by Liquid Metals

a. Polarization Studies in Liquid Metal Environment. Investigation has continued of the occurrence of relatively bare spot areas of small diameter on zirconium surfaces otherwise blackened by exposure to oxygenated sodium at 540°C.

The presence of such spots after exposure for 20 hr has been more definitely associated with moisture picked up during transfer of sodium to the cell prior to test. When a cell loading was carried out in a helium dry box, the subsequent test exposure resulted in a sample surface uniformly coated with black film. There was some evidence suggesting the existence of lighter spot areas at some time before removal. A second experiment with the same sodium load again gave a surface free of the relatively bare spots. These results were similar to those reported previously after application of a vacuum gas-extraction technique to a different sodium load.

The vacuum-extraction technique, however, has not always produced sodium in which uniform sample surfaces were afterwards obtained. This is presently attributed to variations in the amount of moisture picked up during what has been the normal transfer process (under argon blanket with some momentary exposure to room air). Present effort is directed toward improvement of the dry-box atmosphere to permit sodium transfer with a minimum of contamination.

Measurements of rate of hydrogen removal by the vacuum-extraction technique verify that either prolonged pumping (see Progress Report for January 1965, ANL-7003, p. 45) or dry-box loading results in lower rates of hydrogen extraction, implying lower hydrogen concentration in cell sodium as a result of either process.

b. Dissolution Kinetics in Liquid Metals. The first of a series of dissolution experiments in the Ta-Sn system has been performed in which the rotating-disc sample configuration was used. Tin samples obtained during the course of the dissolution run have been analyzed for tantalum by the neutron-activation method. The results indicate that the sensitivity of the method will be adequate to obtain dissolution rate data over a wide range of temperatures. A series of experiments are in progress to determine the temperature dependence of the dissolution rate at a fixed Reynolds number.

4. Plated Coating as a Deterrent to Oxidation of Refractory Metal

When a refractory loop is operated at high temperature in an inert atmosphere, the loop slowly disintegrates by oxide scaling. Complete removal of moisture and oxygen from the inert gas is extremely difficult without an extensive system of cold traps. In order to prolong the life of the loop by removing minute concentrations of oxygen, nickel has been plated on the refractory metal surface followed by high-frequency heating to secure adherence.

Six Nb-1% Zr samples which have been coated with 0.5-mil nickel by the electroless process were exposed to thermal-cycling tests. Two were not heat treated and two were subjected to three 4-sec rf pulses which raised the samples to 1530°C. The remaining two were treated to 30 cycles to the same temperature. These six samples were cycled to 1500°F once a day for 12 days. At the end of this time, five of the samples remained unchanged. The sixth showed a slight flaking of the coating.

D. Other Reactor Fuels and Materials Development

1. Nondestructive Testing

a. Determination of Elastic Moduli of High-temperature Materials by Ultrasonics. The object of this program is to measure the temperature dependence of the elastic moduli of materials that show promise in high-temperature reactor applications. To obtain these data a vacuum furnace has been constructed in which solid bar-shaped samples will be mounted. Pulsed ultrasonic waves will be propagated along the length of these samples, and the transit times of pulses passing a heated, indexed region in each bar will be measured. The indexing is done by machining one end to a smaller diameter than the rest of the bar.

The velocity of sound in the indexed region can then be calculated since one has the length of this region and the transit time in it. Both shear wave velocities and longitudinal velocities are determined. Any of the elastic moduli, e.g., Young's modulus, Poisson's ratio, shear modulus, can be determined if the sound velocities are known.

The flange that will hold the sample bars in a high-temperature furnace, known as a "Brew" furnace, was tested in that furnace. A stainless steel rod was placed in the specimen port so that its indexed end was in the hot zone of the tantalum-sheet heater. In order to test the efficiency of the cooling jacket, the sample was taken up to 1450°C (near the melting point of the bar). The top end of the rod remained cold. The bar was brought back to room temperature.

Subsequently, a 5-Mc quartz crystal was coupled to the bar and 5-Mc, 1/2-μsec pulses of sound were sent down the rod during a second heating run. The echoes were detected, amplified, and displayed on the oscilloscope. It was noticed immediately that the echoes were very weak as compared with echoes previously observed in the same specimen, and that the noise level of the system had increased. The echo signals were observed until the bar was brought to near its melting point, when they disappeared.

After the bar had cooled, different transducers operating at different frequencies were tried. Echoes were observable at 1 Mc and at 2.25 Mc; at 5 Mc, the ultrasonic noise level of the system (which increased with increasing frequency) was higher than the echo signal. The results of these and other tests indicate that the heat treatment given the bar caused the grains in the heated region to grow. The 5-Mc sound was scattered so that only a small percentage of the total sound energy reached the end of the bar in a coherent form. Since 2.25-Mc sound got through the bar in a coherent form, it is thought that the grain size probably approached the wavelength of 5-Mc sound in steel, namely, 0.12 cm.

Measurement of the temperature of the index region of the bar while it was mounted in the Brew furnace would be rather difficult, particularly the measurement of any thermal gradient in the index region. For this reason, a mirror is being built into the lower flange of the furnace so that the specimen can be viewed from the bottom. This way the temperature

of both the shoulder (at the junction of the large diameter part of the bar with the index region) and the end of the bar can be measured optically. The temperature difference between these two regions is the temperature gradient in the index region.

b. Correlation of Sound-transmission Properties and Bond Quality. An analysis of the thermal conductivity K and ultrasonic transmission data for copper braze-bonded specimens has been completed. A point-by-point (1-mm^2 area) comparison of thermal and ultrasonic measurements was made, as well as a comparison of overall ultrasonic transmission with average thermal conductivity in 7-mm^2 areas.

The results show that ultrasonic transmission decreases with a decrease in thermal conductivity, but that the rate of decrease of the ultrasonic transmission is strongly frequency dependent. For the copper braze-bonded specimens when K is either 0.735 or 0.283 of the standard value (K_{std}), the amplitude A of ultrasonic transmitted pulse as compared with the standard (A_{std}) is given in Table XV. When K/K_{std} falls to 0.01, no effective transmission occurs at any frequency. The results for roll-bonded specimens are similar, although not as detailed, as the lowest value for K/K_{std} was 0.890.

Table XV. Relationship of Thermal Conductivity to Ultrasonic Transmission as Affected by Frequency

K/K_{std}	Ultrasonic Frequency, Mc	A/A_{std}
0.735	1.0	0.82
	2.25	0.12
	5.0	0.045
0.283	1.0	0.25
	2.25	0.03
	5.0	0.02

c. Development of a Neutron-image Intensification System. A television system in conjunction with a neutron-image intensifier was used in a postirradiation annealing study of an irradiated fuel pin. The neutron transmission image of the fuel pin, through the stainless steel tube, and tantalum and alumina containers around the pin, and through the furnace, was continuously observed on the television monitor for about 5 hr. Motion-picture records were made periodically, and the entire run was recorded on video tape. Upon heating, the fuel expanded, the cladding ruptured, and fuel spilled out, collecting at the bottom of the alumina crucible immediately surrounding the jacketed fuel.

From the standpoint of the detection system, this first attempt was reasonably successful. The equipment functioned well during the entire run. However, a number of modifications will be made before a second run is made.

The thickness of the furnace should be changed. Under the conditions used for the first run, it was impossible to place the fuel pin closer than about 7 cm from the window of the image-intensifier tube. The internal spacing of the target inside the tube added another 1 to 1.5 cm. At that distance between object and detector, the divergence of the beam produced a picture that lacked the desired resolution. A thinner furnace and a new image-intensifier tube in which the target-to-window spacing will be reduced should alleviate much of that problem. Such an intensifier tube is now being assembled by the Rauland Corp.

The playback quality of the video tape recording was very poor, a great deal of noise being evident. Possible causes for this are now being studied. Fortunately, the motion-picture recordings made directly from the kinescope on this first run were of good quality, and therefore yielded a good record of the run.

E. Engineering Development

1. Development of Manipulators for Handling Radioactive Materials

a. Electric Master-Slave Manipulator Mark E4. A mockup of one of the master-arm configurations designed to use metal tapes instead of cables to drive some of the motions (see Progress Report for January 1965, ANL-7003, pp. 48-50) has been made. Because of this, the configuration of the master arm must be different than that of the slave. In the mockup, the master arm is similar to the slave arm from the wrist joint to the shoulder joint. However, the arrangement of the servo drive units is different in order to provide a straight run of the tapes from the lower arm to the servo drive units. These master arms are designed to be supported by a floor-supported vehicle.

Tests have been carried out to determine the amount of "cross talk" between one motion and another. With a 500-ft unshielded cable between master and slave, one motion moving about $2\frac{1}{2}$ in. can cause another motion to move 0.030 in., which is an acceptably low amount of cross talk. The final judgment, however, must wait until the entire manipulator is assembled and tested as a complete unit If, in the final unit, the cross talk interferes with performance, it can be reduced considerably by utilizing a step-down transformer in the position circuit or by using a shielded cable.

Design and testing work on other components and subassemblies is being continued.

b. Improved Manipulator Tongs or "Hands." Several configurations of 3-fingered "hands" are being investigated in which the shape of the fingers could be rapidly changed, either by master-slave motions or through switch-operated drives (indexing). It may prove to be desirable to change the shape of the fingers by indexing and then apply the grasping or "squeeze" force through a force-reflecting servo. Such a system would retain the force-reflecting squeeze capabilities of present manipulators without the cost and complexity of master-slaving each of the finger motions.

2. Two-phase Flow

a. Void-fraction - Pressure-drop Facility. The loop has operated approximately 3500 hr at temperatures above 1000°F, including approximately 700 hr at boiling temperatures between 1350 and 1650°F, the

maximum sodium temperature to date. While operating at 1650°F, a thermal-stress failure occurred in the condenser above the free sodium surface, releasing a small amount of sodium vapor to the atmosphere. The loop was immediately shut down, and repairs were effected while maintaining an argon gas purge above the sodium level. Contamination of the sodium has most certainly occurred, however, and it is not known how much longer the loop will operate with its present charge of sodium. The loop is being heated slowly to test the condenser repairs. If failure reoccurs, the sodium will be hot-dumped and the condenser removed for more complete repairs.

The data derived from these experiments has not been thoroughly analyzed, but some qualitative observations may be made. Because of the homogeneous boiler, no large liquid superheats are needed to initiate boiling, i.e., the boiling here is not a surface phenomenon, so that nucleation occurs in a manner not defined by the usual surface nucleation theory associated with channel boiling.

With respect to variation of vapor volume fraction and pressure fluctuations, boiling is highly unstable in the low-pressure range (2-7 psia). Stability increases markedly with increases in boiler power density, flow rate, and loop pressure. These boundaries are being defined quantitatively for the loop configuration under study.

It appears that slip ratios are decidedly higher than those predicted by correlations derived from water and other lower-temperature data; however, it should be noted that these sodium experiments have been performed in a very low-quality range, and the values of pressure and density ratio are, in general, outside the recommended usable range of such correlations as proposed by Lockhart-Martinelli and Marchaterre-Hoglund.

These experiments will be terminated shortly. The operating life of the facility at temperatures above 1500°F is short, due to materials limitations. Future use of the loop will be limited to instrumentation studies and calibrations.

3. Boiling Liquid Metal Technology

a. Niobium-1% Zirconium Loop. The Nb-1% Zr loop construction schedule is still proceeding as planned. Pratt & Whitney-CANEL reports that it may be possible to machine the boiler section as originally designed. At the present time, it is planned to attempt both the extrusion method and the deep drilling method for boiler fabrication. Some final changes in loop design have been effected, and a complete review of the design and fabrication procedures will be made in conjunction with P & W staff during the next reporting period.

Construction of the loop support structure and procurement of the tantalum shutter material are underway, covering the following items: sodium loop support, sodium loop heater, sodium loop preheater, experimental shutter design. A die has been fabricated to form the necessary corrugations in the shutter plates.

Most of the cooling-water circuits associated with the vacuum chamber have been installed, complete with the flow and temperature instrumentation and interlock circuitry. Several methods for drain-water disposal are being considered. It is planned to discharge the immediate requirements of about 5 gpm into the laboratory drain until a permanent solution is found for higher flow rates.

The chamber-seal vacuum line has been fabricated, leak checked, and installed. Some necessary steel reinforcements were added to the chamber walkway. Hardware for supporting the sodium pump stator was selected and ordered. A supporting stand has been designed for service as a storage and cleaning station for the chamber bell jar, and materials for this are being assembled. A survey of cleaning fluids suitable for use with the vacuum chamber was made, and some solvents have been obtained. A mass-spectrometer leak detector has been received, given an initial checkout and servicing, and will soon be ready for use. Panels for the switchgear and controls for the sodium pump are being designed. Some of the switchgear and instrumentation for the pump have been received; part of this equipment is improperly sized, however, and will be exchanged.

Design and fabrication of the pressure transducer assemblies is still in progress. Final selection of the thermocouple designs is still undecided, because of material and vacuum-operation incompatibilities. The calibration facility will utilize a high-temperature vacuum furnace, now being installed in D-208.

b. Heater Experiments

(i) Thermal Radiation Heater Experiment. The purpose of the thermal radiation NaK loop is to investigate thermal radiation as a means of transferring heat to and from a flowing liquid metal loop, to test some of the hardware associated with liquid metal experiments, and to observe the behavior of a boiling liquid metal flow loop. The thermal radiation heater has operated 750 hr at temperatures up to 1400°F, heat fluxes to 62,000 B/hr-ft^2 and flow rates up to 416 lb/hr. All loop components have performed satisfactorily.

A complete discussion of both the single-phase and boiling heat transfer observations together with results will be reported in a forthcoming topical report.

(ii) Electron-bombardment Heater Experiment. The basic purpose of this experiment is to experimentally investigate electron-bombardment heating as a means of supplying high heat fluxes to high temperature liquid metal systems. It is also expected that basic information concerning pool boiling from a cylinder may be obtained. A brief description of the electron-bombardment heated experiment is found in the Progress Report for August 1964 (ANL-6936, p. 59).

The high-voltage regions of the experimental facility have been fenced in. Modification and calibration of the instrumentation is nearing completion. Failure of a supplier to ship a voltmeter and an ammeter on schedule will delay operation of this experiment by several weeks.

4. General Heat Transfer

a. Heat Transfer in Double-pipe Heat Exchanger

(i) Liquid Metal Cocurrent Turbulent Flow. Heat transfer tests with the nickel test section having a heat transfer length of ten diameters have begun. Repeated attempts to copper-plate the test section prior to installation into the loop failed. Treating the section with a 50% solution of hydrochloric acid followed by agitating the test section when filled with mercury appeared to promote sufficient amalgamation of the nickel to eliminate wetting problems.

First tests gave large heat-balance deviations, especially across the water cooler. Use of a constant-head tank and a pump system to maintain a steady water flow together with a relocation of the thermocouple to measure the bulk fluid temperature of the mercury leaving the cooler, lowered the heat balance deviation from 15-20 percent to 0-4 percent across the cooler. Heat balance errors of the order of 8% across the test section indicate the necessity to relocate the thermocouples used to measure the bulk fluid temperatures of the mercury exiting from both the tube and annulus of the test section.

Heat exchanger efficiencies have been obtained which are approximately 20 percent over those predicted analytically. Calculation of heat exchanger efficiencies according to conventional analysis under assumed boundary conditions of a constant-temperature wall yields efficiencies which are about 40 percent below those obtained experimentally.

It is believed that a significant amount of heat is being conducted across the end plates at the two ends of the exchanger, which results in an additional heating of the annulus side fluid. This is borne out partly by a circumferential temperature variation on the outside wall near the annulus outlet. The ratio of the annulus-side to tube-side local Nusselt numbers at the end of the section is higher than expected, which is also indicative of significant heat conduction across the end plates of the exchanger.

The heat exchanger analysis suggests a procedure for determining the local overall heat transfer coefficient at the end of the exchanger when the heat transfer is fully developed. The procedure requires a measurement of the temperature distribution along the length of the outer wall of the annulus. These temperatures, after being properly nondimensionalized, are plotted on semilog graph paper as a function of the heater exchanger length. When the heat transfer is fully developed, the plot yields a straight line, the slope of which is proportional to the fully developed heat transfer coefficients. Preliminary calculations have shown that the heat conduction across the endplates results in a distortion of the temperature profile along the length of the exchanger. During these preliminary runs, it has proven difficult to determine the overall heat transfer coefficients from the outside wall-temperature distribution.

While tests continue with the present test section, the longer test section (20 L/D heat transfer length) is being reworked to reduce the heat conduction across the endplates. When the new test section is installed in the loop, the thermocouples used to measure the bulk fluid temperatures at the tube and annulus exits will be relocated. It is expected that tests with the new test section will begin within several weeks.

5. ANL-AMU Program

Other heat engineering experiments, performed as part of a joint program (not supported by the Division of Reactor Development and Technology) between the Laboratory and the Associated Midwest Universities (AMU), are described below.

a. Heat Transfer Instabilities near the Thermodynamic Critical Point. Previous progress reports have described the rapid acoustic type of oscillations which were encountered during heat transfer to a fluid at a supercritical pressure, but with a bulk temperature substantially below the critical temperature. A second type of oscillation was encountered as the bulk temperature approached the critical temperature.

This oscillation is characterized by a frequency two orders of magnitude slower than for the acoustic type. Instead of acoustic pressure waves propagating around the loop, this type of oscillation is analogous to consideration of the fluid in the loop as a solid body performing a mechnical vibration about the equilibrium position. If not periodically perturbed, such a vibration, similar to that performed by a U-tube manometer, would quickly damp out due to the natural damping forces. The data indicate that the perturbing force, or forcing function, is caused by a sudden change in the heat transfer coefficient under certain conditions. The sudden improvement of the heat transfer coefficient is attributed to the occurrence of a "boiling-like" phenomenon in the supercritical fluid.

Both types of oscillation also occur during subcritical boiling heat transfer. Generally, the acoustic type is considered of secondary interest, but a large amount of attention has been focused on the second type of boiling-instability studies. Boiling instability is still not well understood, perhaps because of the lack of a satisfactory physical explanation of the phenomenon. The results of the present supercritical studies contribute an insight into the physical nature of the instabilities, which should be applicable for both sub and supercritical systems.

A record of the experimentally observed behavior during the slow oscillations is shown in Figure 17. When the heat transfer coefficient improvement, or "boiling-like" phenomenon occurred, the wall temperature dropped rapidly, as approximately indicated by the insulated thermocouple on the outside wall. The suddenly decreased wall temperature caused the net heat transfer to increase rapidly even though the electrical power to the test section remained constant. If the 0.035-in.-thick heater wall was cooled 45°F in 2 sec, the heat transfer rate to the fluid was doubled at 8-kW electrical power input. The suddenly increased heat transfer rate caused a rapid expansion of the fluid in the test section, resembling a mild flashing, and caused the observed pressure pulse. The expansion of the fluid in the heated section and riser contributed to a greater density head, which is the driving force of the free-convection flow rate. This caused the flow rate to increase suddenly. After rising to a maximum, the flow rate decayed asymptotically. The asymmetrical shape of the sustained flow oscillations is characteristic of the results of many other instability studies. Such a shape indicated that a perturbing force is affecting the system, resulting in an increased time derivative of the flow rate while it is effective. If the "boiling-like" phenomenon was not repeated, the oscillations damped out after only a few cycles, as is graphically illustrated at the end of the record.

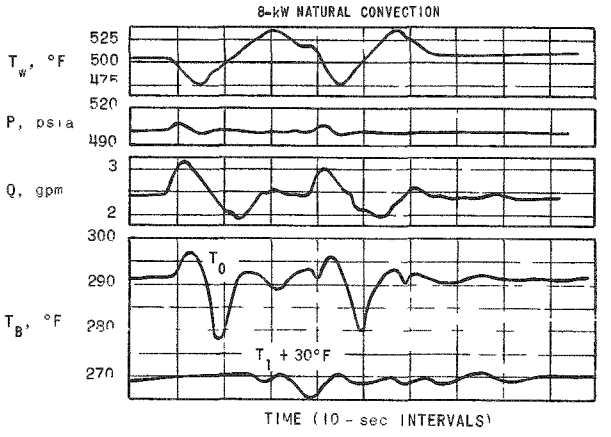

Figure 17. Experimental Record of Slow Oscillations; Wall-temperature Drop in Phase with Flow Oscillations

Figure 17 is an illustration of the heat transfer improvements occurring in phase with the flow oscillations, as frequently happened. Occasionally, the improvements occurred out of phase with the flow oscillations, and the resulting record provided additional insight into the mechanism. When the time between improvements was longer than the flow period, the flow decayed asymptotically back to equilibrium following an impulse, as shown in Figure 18. This record definitely shows that the improvements must be repeated for the oscillations to be sustained.

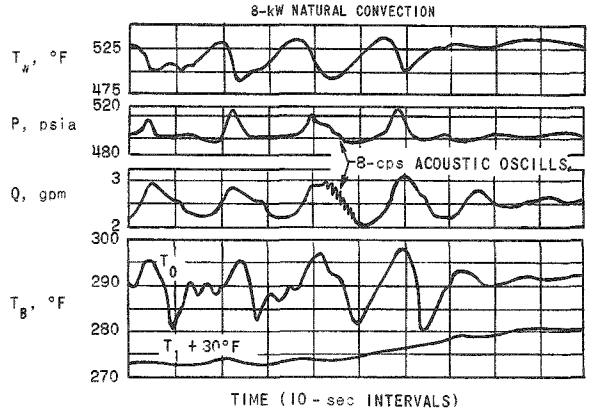

Figure 18

Experimental Record of Slow Oscillations; Wall-temperature Drop Out of Phase with Flow Oscillations

Figure 19 is an illustration of the occurrences when the time between heat transfer improvement is less than the flow period. The effect of a heat transfer improvement out of phase is to cause a pressure impulse, but to not greatly affect the flow rate. The flow rate still tends to oscillate at its natural frequency.

Figure 19

Experimental Record of Slow Oscillations; Wall-temperature Drop Out of Phase with Flow Oscillations

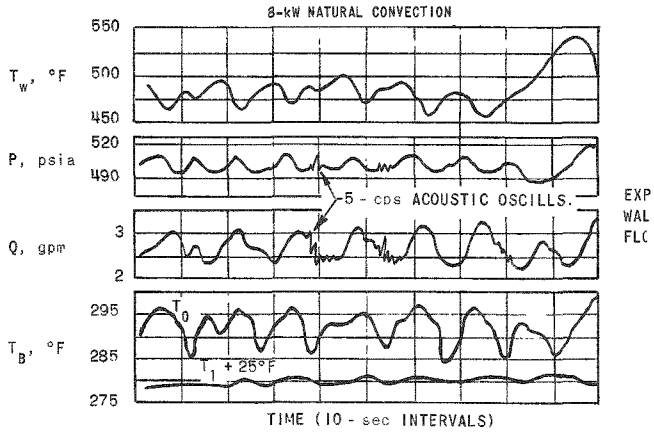

Frequently, the acoustic type of oscillation occurred simultaneously with the slow oscillations, as shown in Figures 17 and 19, which is further proof that these oscillations are of a distinct nature. The reason for the more severe pressure surges in Figures 17 and 19 is that the accumulator valve was barely cracked open. This also resulted in less variation of the inlet bulk temperature than is shown in Figure 18. Results of such tests indicated that the forcing mechanism did not depend primarily upon either the pressure surges or an inlet-temperature feedback.

Work is progressing upon a numerical solution to the problem. The preliminary results demonstrate that the heat transfer coefficient improvement observed is sufficient to result in the observed flow and pressure oscillations.

The factor which caused the "boiling-like" behavior to be initiated must be better understood before an explanation of varying times

between heat transfer improvements can be advanced. Nevertheless, these results clearly illustrate the role of the heat transfer improvement in triggering and maintaining the slow oscillations. It is believed that a similar conclusion holds for subcritical boiling systems. The suddenly increased heat transfer rate as subcooled boiling is initiated may well be the primary forcing function which causes boiling instability to be initiated and sustained, rather than the hydrodynamic characteristics to which the boiling instability is often attributed.

b. Power-to-Void Transfer Functions. The experimental investigation of the void response in a reactor coolant channel as the heat production in the fuel is varied (power-to-void transfer function) has been completed with runs at 800 psia. Both dynamic measurements and axial and transverse steady-state void fraction distributions were obtained at this pressure. For previous results refer to Progress Reports, ANL-6923, July 1964; ANL-6936, August 1964; ANL-6965, October 1964; ANL-6997, December 1964.

At present, the theoretical prediction of the power-to-void transfer function is being carried out employing the "Kjeller Model"[17] which has been programmed for a digital computer using a step-by-step integration procedure. These predictions will be compared with the transient experimental results and also the steady-state axial void distributions in order to determine the degree of agreement between theory and experiment.

c. Two-phase Flow Characteristics during the Complete Vaporization of a Fluid. The Freon loop has been operated with an electrically heated nickel tube ($1\frac{1}{4}$ in. in dia) as a source of vapor generation. A series of tests has been accomplished at a single pressure at the inlet of the unheated rectangular test section, and at various flow rates and qualities. The X-ray unit with fluoroscope has been employed in conjunction with a television monitor for viewing the various flow regimes. Simultaneously, a gamma-ray traverse has been taken at several vertical positions along the unheated section. Local pressure drops along the unheated section have been recorded by means of a transducer-strip recorder arrangement. Several burnout points have also been noted.

The X-ray unit has provided a view of flow regimes which included the bubbly, the slug, the churn, and the annular regimes. The transition between these regimes is not clearly defined with the exception of the transition between the unsteady-type annular flow to that of a steady type. The steady-type annular flow is characterized by the absence of large wave fronts in the liquid film and a corresponding steadiness in the local pressure drops. The results thus far for the transition of these two types of annular flow are reproducible and have appeared quite regularly

[17] Solberg, K. O., The Kjeller Model for the Dynamics of Coolant Channels in Boiling Water Reactors Part I: Theory, EAES Symposium, Studsvik, Sweden (Oct 1963).

with varying flow rates at a fixed system pressure. The void fractions obtained thus far for the steady annular regime are of the order of 90%. The slug-annular flow transition is not distinct; however, the results obtained thus far are in the same order of magnitude as for water when the comparison is made on a similarity basis.

Construction of a flow-regime map for the single test pressure is being undertaken in order to establish the guides for further tests at more elevated pressures. This series of tests should be completed within a month.

F. Chemical Separations

1. Fluoride Volatility Processes

a. Recovery of Uranium from Low-enrichment Ceramic Fuels

(i) Laboratory Support Work. Laboratory work in support of the pilot-plant investigation of the fluid-bed fluoride volatility process has continued. In the fluid-bed fluoride volatility process, fluorination of UO_2-PuO_2 fuel is conducted in the presence of granular alumina. Since the alumina will be ultimately discarded as waste along with associated fission products, it is essential that very little uranium and plutonium be retained on the solids after fluorination. Experimental work in a $1\frac{1}{2}$-in.-dia fluid-bed reactor (see Progress Report for November 1964, ANL-6977, p. 67) has shown that it is possible to achieve overall plutonium recoveries of greater than 99% by reuse of the alumina bed. A preliminary study was made to determine the efficiency of removal of the small amount of plutonium retained on the alumina by leaching with nitric acid. Recovery of plutonium by acid leaching of the alumina is not expected to be a process operation, but was investigated only as a backup procedure in the event that some malfunction should prevent removal of plutonium by the fluorination method.

Alumina beds containing plutonium from previous fluorination experiments were used in the leaching tests. In each test, 50 g of alumina bed was slurried with 100 ml of a leaching solution containing 6N nitric acid and 0.1M aluminum nitrate. After a leaching period of 5 hr at 100°C, between 80 and 90% of the plutonium present on the alumina was leached from the solid. In tests in which a bed material containing 0.118 w/o plutonium was leached with the nitric acid solution, the plutonium concentration on the alumina was reduced to approximately 0.01 w/o. In similar tests with a bed material containing 0.011 w/o Pu, 0.014 w/o U, 3.3 w/o Fe, and 0.32 w/o Cr, the final plutonium concentration of the alumina was approximately 0.002 w/o. About 85 to 90 percent of the chromium and iron was also removed from the alumina bed by the leaching solution.

(ii) Decladding and Fluorination Experiments. In preparation for tests with plutonium-containing feed material, eleven runs were performed in the 2-in.-dia reactor with UO_2 fuel. Two processing techniques were evaluated in these runs: (1) a chemical pulverization of UO_2 pellets by reaction with $HF-O_2$ mixtures to form a powdered mixture of UO_2F_2 and other compounds, followed by fluorination of the mixture to recover the uranium as UF_6; (2) a two-zone oxidation-fluorination procedure in which UO_2 pellets in the lower zone are reacted with oxygen to form U_3O_8 fines which are transported to the upper fluidization zone where they are fluorinated to UF_6 with fluorine.

Initial tests in the 2-in. reactor (see Progress Report for December 1964, ANL-6997, pp. 40-41) involved the investigation of the behavior of UO_2 pellets during reaction with $HF-O_2$ mixtures (40 v/o HF, 60 v/o O_2) at 400 to 550°C, and the recovery of UF_6 by fluorination of the products of the reaction. The reaction between UO_2 and $HF-O_2$ mixtures resulted in the formation of fine particulate material which was readily elutriated from the fluid bed into the upper sections of the reactor. A fluid-bed reactor, designed specifically to reduce the number of inclined surfaces in the disengaging and filter sections on which fine particles might accumulate, has been installed in the plutonium facility.

It was also observed in the previous tests that caking of a portion of the fluid bed frequently occurred during the $HF-O_2$ reaction step. Satisfactory operation, as determined by the absence of caking, was only achieved in tests in which the UO_2 pellets were contained in an open basket immersed in the fluid bed. Caking of the pellets and alumina bed material has been avoided in recent tests by operating with reduced reactant concentrations in the fluidizing gas. Satisfactory pulverization of a 2-in.-deep bed of UO_2 pellets was obtained using 20 v/o HF-30 v/o O_2 in nitrogen at 450°C. Operating under these conditions, the pellets in a 2-in.-deep bed were completely pulverized in 3 hr. A two step procedure was then successfully employed for fluorination of the reaction products: (1) fluorination for 3 hr at 450°C with 3 to 15 v/o F_2 in nitrogen without recycle; (2) fluorination for 5 hr at 450°C with 80 to 95 v/o F_2 with continuous recycle.

In a run using the two-zone oxidation-fluorination technique in the 2-in.-dia reactor (see Progress Report for January 1965, ANL-7003, pp. 58-59), a 2-in.-deep bed of sintered UO_2 pellets was immersed in a 12-in.-deep bed of -48 +100 mesh alumina particles. The conditions employed in this run were chosen to simulate those to be used in runs with plutonium-containing fuel materials. A total of 100% of the uranium was collected as UF_6 in the product recovery system, and the final concentration of uranium in the alumina bed at the end of the run was less than 0.01 w/o. No processing difficulties were experienced during the run.

Development work in the 3-in.-dia pilot-scale reactor has continued on establishing optimum processing conditions for decladding and

fluorinating uranium dioxide fuels. Current work has been concerned with the processing of Zircaloy-2-clad UO_2 fuel. A run was made in the pilot-scale reactor to determine the feasibility of processing Zircaloy-2-clad UO_2 fuel bundles by destructive oxidation with $HF-O_2$ followed by fluorination to recover the uranium as UF_6. The progress of the reactions was observed during this run by γ-ray photography. Current plans are to declad Zircaloy-2-clad UO_2 fuels by treatment with HCl to form volatile $ZrCl_4$, and the destructive oxidation procedure is considered as an alternative method.

A simulated fuel bundle, comprising six 2-ft-long Zircaloy-2 tubes packed with cylindrical UO_2 pellets (0.43 x 0.43 in.), was charged to the fluid-bed reactor. The total charge consisted of 3.2 kg UO_2 and 0.92 kg Zircaloy-2. The inert fluid-bed material was 5.5 kg of -48 +100 mesh alumina particles.

The decladding conditions employed in this run were similar to those established previously in bench-scale studies (see Progress Report for January 1965, ANL-7003, p. 58). Decladding was conducted for $6\frac{1}{2}$ hr at 550°C with a gas mixture containing 45 v/o HF in oxygen. Operation during the first 3 hr proceeded smoothly. However, during the final $3\frac{1}{2}$ hr of the decladding step, the bed temperature decreased to 300°C because of poor heat transfer, although the reactor wall temperatures remained constant throughout the entire period. Apparently, disintegration of the Zircaloy tubing produced a scaly oxidation product which restricted movement of the fluidized-bed particles and thus caused a marked reduction in heat transfer from the reactor wall to the center of the bed.

Fluorination was conducted with the use of a fluorine feed system designed to facilitate fluorination of the large quantity of uranium fines in the bed. During the initial fluorination period ($2\frac{1}{2}$ hr), fluorine and recycle gas were introduced into the side of the reactor at approximately the middle of the fluid bed, and nitrogen as the fluidizing gas was fed at the bottom of the reactor. During the subsequent 0.5-hr period, the fluorine and recycle gas were introduced through a side inlet located 10 in. below the first inlet. The fluorination step was completed by introducing fluorine and recycle gas at the bottom of the reactor for 6 hr. Throughout the entire fluorination step, the temperature of the fluid bed varied widely (between 300 and 850°C) due to the poor fluidization properties of the bed. High UF_6 production rates [50 lb/(hr)(sq ft)] were achieved during the initial 2 hr of fluorination, wherein 56% of the uranium was recovered as UF_6.

At the end of the fluorination step, large cakes containing ZrF_4, AlF_3, and Al_2O_3 were found in the reactor. No uranium compounds were detected in the cakes. A factor which may have contributed to the formation of the cakes was that the fuel bundle was not completely oxidized at the time the fluorination step began. This was observed in the γ-ray

radiographs taken at several intervals throughout the run. A radiograph taken at the start of the fluorination step showed the presence of unreacted UO_2 pellets.

Further work on the destructive oxidation method for decladding Zircaloy-2-clad UO_2 fuel is being conducted at other laboratories.

(iii) Supporting Studies on Fluidization of Fine Particles. In the decladding of UO_2 fuel with gaseous mixtures of $HF-O_2$, the oxide fuel reacts with the decladding agent to form a powdered mixture of UO_2F_2 and and UF_4. The production of a large quantity of this fine material greatly affects the behavior of the fluidized bed. The minimum fluidization velocity (the gas velocity at which fluidization of the particles starts) is markedly reduced, and a large fraction of these particles is elutriated from the fluidized bed into the upper sections of the reactor. Studies of the behavior of fine particles in fluid-bed reactors are under way to assist in the process development program on the pulverization of UO_2 fuel.

In preliminary fluidization studies in a 2-in.-dia Lucite reactor, the minimum fluidization velocity of -48 +170 mesh alumina was determined to be 0.19 ft/sec. The minimum fluidization velocity was reduced to 0.05 ft/sec by the addition of 25 w/o fines (uranium oxides and fluorides). With continued fluidization of this mixture, it was observed that bridging of fine material in the upper section of the reactor occurred between a sintered metal filter and the wall of the reactor. This behavior indicates that a large portion of the fines may accumulate in the upper portion of the reactor unless special techniques are incorporated to return them to the bed. Blowback of the filter by a reverse flow of gas through the filter was effective in returning to the bed the fines which had accumulated on the surface of the filter.

A series of tests have been performed to determine the manner in which fine particles are distributed in a fluid bed of -48 +170 mesh alumina. A quantity of -325 mesh uranium fines (UO_2F_2 and U_3O_8) was added to a bed of alumina to give a mixture containing 40 w/o uranium fines. The bed was fluidized at a gas velocity of 1.0 ft/sec and samples of the bed were taken at various levels and the fines content was measured. The results revealed no distinct separation of fines and coarse particles although there was a variation in fines concentration with height. Fine particles were more concentrated at the top and at the bottom portions of the bed than at the center. These tests indicate that a distribution of fine particles would occur in the bed satisfactory for conducting fluorination reactions, and that if a portion of the bed became depleted of uranium by fluorination, fines would be transported into the depleted portion. Further tests are planned to determine the optimum particle size distribution which would result in a more uniform concentration of fines in the bed.

2. General Chemistry and Chemical Engineering

a. Chemistry of Liquid Metals

(i) Sodium Purification. Previous studies (see Progress Report for January 1965, ANL-7003, p. 24) of the chemistry of carbon in sodium have revealed that a large proportion of the carbon in nominally pure sodium is present as particulate, carbonaceous material. Further insight into the nature of the particles is being sought by the use of filtration, centrifugation, optical and electron microscopy, autoradiography (after labeling carbon with ^{14}C), and exchange reactions with ^{14}C-labeled carbon compounds. Recent results obtained with the first two techniques are discussed below.

Several different filtering materials and filter combinations have been tested for removal of particulate carbonaceous material from liquid sodium at about 150°C. These include (a) 1.2-μ-porosity Millipore* filters (cellulose plastic porous membrane type), (b) sintered carbonyl nickel filters (<5-μ porosity), and (c) 5-μ-porosity stainless steel filters in combination with activated charcoal. Some lowering of the carbon content was achieved, but, in general, the carbon level after filtration was found to be in the range from 50 to 125 ppm. These results suggest the presence of particles 1 μ or less in size. Attempts to filter liquid sodium at about 150°C through 1- to 3-μ-porosity glass filters under a pressure differential of 3 atm were unsuccessful.

A more efficient removal of particulate matter from sodium may be possible by evaporation of sodium through porous filters. An experiment to test this concept was made by heating sodium to 350°C and drawing the vapors by vacuum through a coarse (20-40 μ) and a medium (10 μ) glass frit in succession. The sodium which condensed was found to contain 77 ppm carbon as compared with an original 160 ppm. Similar evaporation-filtration experiments are in progress using stainless steel filters which are capable of removing 0.7- to 1.8-μ-sized particles.

Additional evidence for the existence of submicron-sized carbonaceous particles was obtained by centrifugation experiments. Sodium heated at 200°C in stainless steel capsules was centrifuged for one hour at 2000 rpm (between 335 and 625 G, respectively, at top and bottom of sodium column). The sodium was then allowed to solidify while being centrifuged. Analyses for carbon in the top and bottom 1/4-in. portions of the sodium column showed no significant carbon displacement. Theoretical calculations, however, indicated that for small density differences (~0.2 g/ml) between the particles and the sodium and for 1-μ-sized particles, separation should have been possible under the conditions of centrifugation.

---

*Millipore Filter Corp.

This leads to the conclusion that the carbonaceous particles are smaller than 1 μ; accordingly, work on separation of carbon from sodium by centrifugation is being discontinued.

b. Determination of the Critical Constants of Alkali Metals. The critical constants of a metal can be used for calculating or estimating many thermodynamic and physical properties of the metal. Thermodynamic properties of alkali metals are of particular interest because these metals are used as heat exchange media in nuclear reactors.

Studies to determine the critical constants of alkali metals have been continued with sodium. The high-temperature vapor and liquid density of irradiated sodium containing ^{24}Na have been measured by a radioactive counting technique (described in Progress Report for January 1965, ANL-7003, p. 61) in order to determine the critical temperature of sodium. The estimated critical temperature, based on data to 1754°C, is between 2200 and 2400°C, and the estimated critical density is between 0.18 and 0.21 g/cm^3. Additional runs will be made with irradiated sodium to replicate the results and to obtain data nearer the critical point. Experiments with irradiated potassium are being planned.

c. Preparation of Uranium Mononitride-sodium Paste. Mobile blanket fuels for fast breeder reactors show promise of reducing reactor downtime for fuel shuffling, improving utilization of the sodium coolant and, thus, power conversion efficiency, and decreasing fuel-processing and refabrication costs. Experimental work is under way to develop a paste blanket fuel consisting of a ceramic fuel dispersed in a liquid metal. Currently, the most attractive of the mobile blanket fuels that have been considered is a paste of uranium mononitride (UN) in sodium.

In preliminary studies of paste preparation (see Progress Report for December 1964, ANL-6997, p. 46), wetting of UN powders by sodium was reported. In current experiments, UN powder was heated with sodium at various temperatures in an alumina crucible. Wetting of the UN by sodium was clearly achieved at 300 to 500°C after 1/2 hr of stirring; at 250°C, 1 hr of stirring was required. No instances of dewetting of the UN on cooling were observed in any of these experiments.

Following these studies, preparation of a UN-sodium paste of high uranium content was attempted. The UN powder (~100-μ median dia) with a bulk density of 8.2 g/cc was mixed with sodium at 300°C to obtain 346 g of paste containing 49 v/o solids (6.6-g/cc uranium density). The paste appeared to contain 8-v/o gas as determined by difference from the amounts of sodium and UN added.

At 40-v/o solids, an intermediate stage in the preparation, the paste was judged to have good flow properties. However, in its final composition (49-v/o solids), the paste was quite viscous and probably was

not directly suitable for a flowing system. Additional experimentation is under way to obtain a paste of high uranium density, low gas content, and good flow properties.

d. Calorimetry. Of considerable interest as possible reactor fuels are the phosphides, sulfides, and selenides of uranium. Their enthalpies of formation will be determined by reaction with fluorine. The enthalpies of formation of phosphorus pentafluoride, sulfur hexafluoride, and selenium hexafluoride are necessary auxiliary data whose values have been determined by fluorine bomb calorimetry. (The value for the enthalpy of formation of phosphorus pentafluoride was reported in the Progress Report for November 1964, ANL-6977, p. 72.)

The two-chambered vessel[18] that was developed for substances which react spontaneously with fluorine was used. Samples were supported on nickel dishes for the combustion. Phosphorus pentafluoride was the only product of the phosphorus combustions. Sulfur hexafluoride was the major product of the sulfur combustions; a very small amount of a lower, unidentified fluoride of sulfur was formed, but the thermal correction for this amounted to only 0.004% of the heat evolved. Selenium hexafluoride appeared to be the only product of the combustion of selenium. The enthalpies of formation obtained in these studies are given below:

	$-\Delta Hf^{\circ}_{298}$ (kcal mole^{-1})
P(triclinic, red) + 5/2 $F_2(g) \rightarrow PF_5(g)$	376.7 ± 0.4
S(rhombic) + 3 $F_2(g) \rightarrow SF_6(g)$	291.9 ± 0.3
Se(monoclinic, black) + 3 $F_2(g) \rightarrow SeF_6(g)$	266.8 ± 0.2

The uncertainties given are equal to twice the overall standard deviations. Because the samples used were very pure, the main contributions to the uncertainties were from the precision of the calibration and combustion experiments.

Thermochemical studies on the hexafluorides of the Group VI B elements are to be completed by the determination of the enthalpy of formation of tellurium hexafluoride.

---

[18] Nuttall, R. L., Wise, S. S., and Hubbard, W. N., Combustion Bomb Reaction Vessel for Spontaneously Combustible Materials, Rev. Sci. Instr. 32, 1402 (1961).

G. Plutonium Recycle Reactors

1. EBWR Facility

The field inspection of the EBWR primary plant (see Progress Report for December 1964, ANL-6997, pp. 47-48, and Progress Report for January 1965, ANL-7003, pp. 65-67) was completed.

Summaries of the findings are as follows:

a. Steam Piping (10 in., 8 in., and 6 in.). Eighteen of 31 welds (58%) are sound for service at 650 psig. Stainless steel welds are readily repairable. As some parts were Kanogen nickel-plated, carbon steel piping welds require a reinforcement type of repair in order to control phosphorus of the nickel plate.

b. Two 6-in. Safety Valve Piping Systems (Original and 80-MW Addition). Twenty-six of 40 welds (65%) are sound for service at 650 psig. Original piping is also Kanogen plated and requires the reinforcement type of repair. The 80-MW addition piping is repairable conventionally, i.e., by cutting, rebeveling and rewelding. Studies are in progress to determine the economics of conventional repair of piping versus reinforcement type of repair.

c. Condensate Piping (8 in.). Seven of 11 welds (63%) are suitable for further vacuum services.

d. Ion Exchange Piping (2 in. and Smaller). A few defective welds were found by the dye-penetrant examination and repaired. Approximately one-half (of 28) forged SS304 globe and check valves were found to contain forging laps, bursts, and cracks. Explorations, by grinding, revealed that the defects were in excess of 1/16 in. in depth.

e. High-pressure Boric Acid Line. Replacement schedule 80 seamless pipe and piping materials are on order.

f. Vessel Cladding. Successive nitrogen gas pressurizations, to 800 psi, of the annulus between cladding and vessel wall revealed numerous cracks, including those previously described as "surface decorations." Five of the eight vertical cladding panels were found to be faulted. Partial explorations of the cracks, of approximately 20-ft total length, revealed that:

(i) The visible crack length was shorter than the actual length, i.e., the cladding cracking apparently originated at the interface and propagated radially inward.

from 21°C to 58.4°C and cooled back to 21°C. Reactivity variations were significantly larger than during normal room-temperature operation, suggesting a possibility of compensating effects between different parts of the system which were not always at equal temperatures. The change of water density with temperature was expected to produce a measurable negative temperature coefficient as described in the preceding paragraph.

Table XVII. Worth Measurements

Sample Description	Thickness of Samples (in.)	Weight of Samples (g)	Ratio of Reactivity Worths: Core 315/Core 615
Boral (B_4C-Al); 22.2 w/o B	0.200	17.859	1.19 ± 0.05
Boron-Stainless Steel; 1.01 w/o B	0.200	53.955	1.33 ± 0.10
Cadmium	0.200	62.703	1.32 ± 0.09
	0.010	3.135	1.66 ± 0.19
Europium Oxide-Stainless Steel; 30.97 w/o Eu	0.156	40.707	1.14 ± 0.05
Gadolinium-Stainless Steel; 0.7 w/o Gd	0.200	56.052	1.51 ± 0.10
Hafnium-Zirconium; 97.5 w/o Hf	0.119	55.131	1.11 ± 0.06
Stainless Steel	0.200	56.869	1.43 ± 0.50
Water	0.200	21.657	0.56 ± 0.20
Uranium-Aluminum; 17.44 w/o U	(a)		1.63 ± 0.50

(a) Sample thicknesses were different for the two cores; the ratio given is the ratio of worths per unit cross-sectional area.

During the final run of the temperature-coefficient measurement, a reactivity drift occurred at 21°C, which was later attributed to swelling of a fuel jacket. One of the twelve control-safety blades failed to insert on the intentional scram terminating the run. Inspection indicated that a fuel jacket, located third from the blade in a parallel plane, had swollen sufficiently to produce a frictional bind between the blade follower and the adjacent fuel

plate which was flexed by the transmitted force. A second swollen fuel jacket was found on subsequent inspection of the entire core.

Preliminary investigation failed to give a clear indication of the cause of failures. The fuel jackets had been closed by electron-beam welding of the three open sides of an envelope folded over each uranium metal fuel foil. The envelope was 0.0025-in.-thick stainless steel and the uranium 0.0044 in. thick. Analysis of the gas found in the swollen jackets indicated that it was approximately 90% hydrogen. Color patterns of the dejacketed fuel are not as distinct as would be expected if there were in-leakage of water, and the expected gain in weight was not found, although a metal-water reaction is a likely source of hydrogen gas.

The two jacketed foils had been in use commencing in the October 1964, 315-fuel-foil loading. Each was swollen to 0.4-in. thickness, compared with a nominal thickness of 0.01 in. Weekly core inspection (removal of each 27-plate fuel assembly) has not revealed another failure.

Consideration of the core structure indicates that six of the twelve control-safety blades are free of any risk of obstruction from similar fuel swelling if this should again occur, and that only one blade is likely to be obstructed by any one fuel failure. Although these two fuel failures were in assemblies adjacent to one control-safety blade, it was not affected, although a neighboring blade was stuck. The difference is in the orientation of the fuel plates which may be either edge-on or in planes parallel to the blades.

It should be noted carefully that failures experienced in the critical-experiment fuel have no bearing on the reliability of the proposed fuel for the AARR proper. The critical-experiment fuel is uranium metal foil encased in thin stainless steel envelopes, whereas the proposed fuel for the reactor proper is a clad plate with a 37% UO_2-stainless steel cermet matrix.

Work with the 615-fuel-foil core has reached a stage where reloading will be feasible as soon as their is sufficient jacketed fuel for a loading of approximately 800 foils.

B. Regenerative EMF Cells

1. Engineering Studies of Bimetallic Cells

A sodium-bismuth cell (without a thermal regenerator) is being operated to define some of the engineering problems associated with cell operation (see Progress Report for January 1965, ANL-7003, p. 74). The cell has now been functioning for over 75 days at operating temperatures from about 540 to 630°C. During this period, the cell has been operated as a battery, with approximately 50 discharge-recharge cycles; there has been no observable decrease in cell performance.

In this cell system, for which the anode is essentially pure sodium and the cathode 25 m/o sodium in bismuth, cell current densities at about 575°C were found to be 40 mA/cm^2 at 0.60 V, 80 mA/cm^2 at 0.56 V, and 160 mA/cm^2 at 0.48 V. The stainless steel cell shows no evidence of deterioration; however, refractory metals such as tungsten will probably be required for the regenerator section of the cell system.

A few comments might be appropriate concerning current densities. In operating a sodium-bismuth or other type of bimetallic cell, a polarization at the cathode caused by the concentration gradient of the anode metal diffusing into the cathode metal takes place. This polarization increases with the current density and could be decreased by agitation or flowing the cathode metal across the cathode space Experimental work on this aspect of the cell has not been done. It has been noted that this polarization is negligible at current densities up to about 160 mA/sq cm (1 Amp/sq in) for a nonagitated or nonflowing cathode. The polarization at the anode is much less than that at the cathode. Hence, in cells with unequal anode and cathode areas, a higher current density can be obtained at the anode (without significant polarization) than at the cathode. As an example, we have operated a cell with a 1/4-in.-dia anode and a 1-7/8-in.-dia cathode at anode current densities of about 500 mA/sq cm at about one-half open-circuit voltage and anode current densities of about 1000 mA/sq cm under short-circuit conditions.

In the case of a cell with a 7/8-in.-dia anode and a 7/8-in.-dia cathode, current densities of about 150 mA/sq cm at one-third open-circuit voltage and 225 mA/sq cm at short-circuit have been achieved.

The engineering prototype cell has a cathode area of about 45 sq cm and has been operated at 160 mA/sq cm at three-fourths open-circuit voltage; over 320 mA/sq cm have been attained at near short-circuit conditions. The electrolyte thickness is about 1 in Reduction of the electrolyte thickness and agitation of the cathode metal would improve the performance.

IV. NUCLEAR SAFETY

A. Reactor Kinetics

1. Fast Reactor Safety

a. Transient Expansion of Irradiated EBR-II Fuel Alloy. Data from TREAT experiments on the transient expansion of two unrestrained and unclad EBR-II fuel-pin segments (see Progress Report for July 1964, ANL-6923, p. 88) have been analyzed. Burnup was about 1.2 a/o for both samples, which were taken from a single fuel pin. One sample of 9.1-cm length was given a transient burst of 69 MW-sec, with a power-peak half-width of the order of 0.5 sec. The other, about 14.6 cm long, was subjected to a "constant-power" burst with integrated power of 99 MW-sec and a duration of about 24 sec. Both pins were run unclad. Linear-motion transducers measured expansion during the nuclear heating.

The 9.1-cm pin had a nominal TREAT heating rate of 1000°C/sec; the longer pin, a rate of 80°C/sec. Neither sample was instrumented for temperature measurements. Sample temperatures were inferred from reactor integrated power data, reactor power calibration factors, and enthalpy data obtained for the fast reactor safety program.[19] Heat lost from the samples to the surroundings (a maximum of 5% of energy input over the time ranges of interest) was estimated.

Expansion data are shown in Figures 20 and 21 for the 9.1 cm and 14.6 cm samples, respectively. Also given for comparison are the expansions calculated from the temperature estimates and data[20] for the

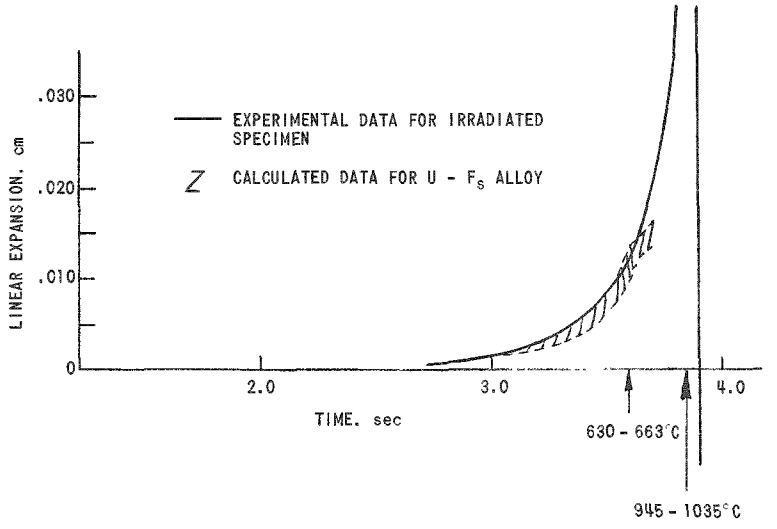

Figure 20
Comparison of Experimental and Estimated Linear Expansion for 9.1-cm Sample, Using Data for Unirradiated U-Fs Alloy

[19] Savage, H., and Seibel, D., ANL-6702 (Sept 1963).

[20] Zegler, S. T., and Nevitt, M. V., Structures and Properties of Uranium-fissium Alloys, ANL-6116 (July 1961).

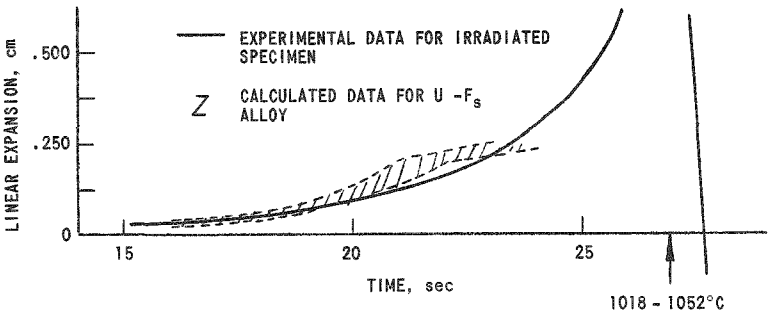

Figure 21

Comparison of Experimental and Estimated Linear Expansion for 14.6-cm Sample, Using Data for Unirradiated U-Fs Alloy

initial out-of-pile heating of an unirradiated U-5 w/o Fs specimen annealed for 11 days at 500°C and water quenched.[21] Because of uncertainties in calibration, a band, rather than a curve, is shown for the calculated expansion. Each band corresponds to an uncertainty of ±10% in power calibration.

The data from both experiments indicate that transient expansion is similar to that for unirradiated material up to about 700°C (the approximate limit of data on unirradiated fuel). At higher temperatures, the transient expansion is appreciably higher than that expected from extrapolations. Expansion for equal temperatures appears to be ~20% lower for the slow-heating-rate excursion than for the high-heating-rate transient. However, this discrepancy is within possible experimental errors for this type of experiment.

Both samples were melted in the course of the experiments. The sharp drops shown at about 3.9 and 27 sec in Figures 20 and 21, respectively, are believed to result from the collapse of the melted specimens. As indicated on the figures, this hypotheses is consistent with the temperature estimates.

b. Transient Experiments on Nb-clad UC Specimens. Four UC elements clad with Nb-1% Zr alloy were investigated for meltdown behavior in TREAT. Each sample consisted of UC, pressed and sintered to approximately 90% of theoretical density. Fuel pellets, 0.648 cm in diameter, were stacked to form fuel cylinders, 27.9 cm long. The cladding was 0.030 cm thick. Irradiation conditions are summarized in Table XVIII.

The samples are being shipped back to Argonne, Illinois for postmortem inspection and analyses.

---

[21] The thermal histories of both the irradiated and unirradiated material are similar. A control sample obtained from the irradiated material prior to exposure in TREAT is available, and structural comparison will be made by metallographic techniques.

Table XVIII. Conditions for UC Irradiation

Sample	Integrated Reactor Power, MW-sec	Estimated Maximum Central Fuel Temperature, °C
1	90.5	1750
2	34.5	900
	56.8	1200
3	121	2350
4	147	2500

c. Meltdown Observation Device for FARET. A study has been made to design the instrumentation for an in-pile loop in FARET to observe fuel movement during fast reactor safety meltdown experiments (see Progress Report for September 1964, ANL-6944, p. 85). The basic design consists of a multichannel collimator system with individual fast-neutron detectors, analogous to that under development for TREAT meltdown experiment. Unlike the TREAT system, which is located outside the reactor shield, the collimator, shielding, and fast-neutron detectors must be placed inside the reactor vessel, requiring operation in a high-temperature, liquid-metal environment. Uranium-238 fission counters are used as neutron detectors in the preliminary design. Estimates now show that performance should be adequate. Since the FARET design requires some steel between the meltdown sample and detectors, some degradation in performance must be expected. Earlier mockup tests at TREAT (see Progress Report for July 1964, ANL-6923, p. 91) have indicated that an acceptable signal-to-noise ratio should be obtained.

d. Ionization of Uranium Vapor during Nuclear Bursts. The effect of ionization on the equation of state is potentially an important mechanism for reducing pressure in the early stages of a severe fast reactor excursion by absorbing energy. In order to test the significance of this effect, the fractional ionization for saturated uranium vapor was calculated from the Saha-Langmuir equation:

$$\frac{\epsilon^2}{1-\epsilon^2} = A\frac{g^- g^+}{g^n}\frac{T^{5/2}}{P}\exp(-I/kT),$$

where

ϵ = fraction of ions;

g^-, g^+, g^n = multiplicities of electrons, ions, and neutrals, respectively;

P = pressure;

T = temperatures, °K;

k = Boltzman's constant = 0.855×10^{-4} eV/°K;

I = ionization potential, eV;

A = constant, 3.27×10^{-7}/atm-°$K^{5/2}$.

The recent value of Mann[22] of 6.11 ±0.05 eV for the ionization potential of uranium was used, and the pressure along the saturation curve was calculated from an extreme extrapolation of the equation of Rauh and Thorn:[23]

$$\log P_{mm} = 8.583 - (23{,}330/T).$$

The multiplicities $g^- = 2$, $g^+ = 9$, and $g^n = 13$ were taken from Katz and Rabinowitch.[24]

Results of the calculations indicate that about 0.3% of the atoms are ionized at the normal boiling point. Even at the estimated critical point:

T_c = 12,500°K; P_c = 6850 atm,

only about 6% of the atoms are ionized. For a reactor excursion which might result in the expansion of uranium vapor to one atomosphere at 5000°K, the fraction ionized after expansion is about 2%.

If the older value of the ionization potential, 4.7 eV, estimated by Rauh[25] were used, the fraction ionized under the conditions above would be larger but still less than 20% for the worst case.

It is hope that similar estimations can be made for plutonium and UO_2. Fractional ionization estimates for UO_2 are considerably more complicated by the dissociation of UO_2 to UO and O_2.

e. Coolant-expulsion Studies (Water). As previously reported (see Progress Report for November 1964, ANL-6977, p. 91), automotive storage batteries are to be used as an energy source in water-expulsion tests. Twenty heavy-duty diesel truck batteries (12 V, 204 Amp-hr) have been purchased and are now installed on a specially constructed rack. The bus-bars are being constructed as are the specially designed battery-terminal clamps. Some of the quartz piping has arrived, and a metal-to-glass seal is being made to hold a pressure transducer flush to the inside wall of the pipe.

---

[22]Mann, J. B., J. Chem. Phys. 40, 1632 (1964).

[23]Rauh, E. G., and Thorn, R. G., J. Chem. Phys. 22, 1414 (1954).

[24]Katz, J. J., and Rabinowitch, E., The Chemistry of Uranium, McGraw-Hill Book Co., Inc., New York (1951).

[25]Rauh, E. G., Work Function, Ionization Potential, and Emissivity of Uranium, ANL-5534 (May 1956).

A representative sample of the stainless-steel test section is being measured to determine the temperature coefficient of resistivity, in order to use the test section as a resistance thermometer.

2. TREAT Operations

Four uranium carbide samples (RP Series 45) clad in niobium were irradiated in transparent capsules and returned to Argonne, Illinois for examination.

Three plutonium carbide samples (MET Series 4) were irradiated and returned to Argonne, Illinois for examination.

Five samples of SNAP fuel were irradiated for Atomics International and returned to Argonne, Illinois for examination.

A mockup of a ZPR-III drawer, containing depleted uranium fuel plates contained in cans of the type to be used for the plutonium fuel for the SEFOR experiments in ZPR-III, was irradiated to measure prompt expansion characteristics. (See ZPPR Section of this report for a summary of results on expansion measurements on ZPR-type fuels.)

3. Large Sodium Loop in TREAT

Assembly of the loop piping has been delayed indefinitely because of delays in delivery of expansion joints and lack of funds to cover welding, X-ray, and insulation costs.

The final parts of the single bellows have arrived from Flexicraft Industries. However, a dye check of the inner ply has shown the presence of a crack in the wall. This portion will be refabricated by the vendor. The Central Shops will concentrate upon the final assembly of these units.

Minor modifications to the gas-system have been proposed to improve the ability to maintain and operate the system. No exceptions were taken to the components currently listed in the bills of material or to the overall design.

Equations of motion have been programmed on an electronic analog computer to investigate the perturbation in coolant flow resulting from energy release to the coolant during a nuclear transient. Because of certain necessary assumptions, the results are valid only for the time interval during which the sodium above the test subassembly is being displaced into the surge suppressor.

V. PUBLICATIONS

Papers

CAPTURE-TO-FISSION RATIOS OF U^{233}, U^{238}, AND Pu^{239} IN EBR-I, MARK III

C. E. Crouthamel, D. C. Stupegia, C. M. Stevens, and Peter Kafalas
Nucl. Sci. Eng. 21, 179-185 (Feb 1965)

LATERAL TRANSPORT IN A FLUIDIZED-PACKED BED. PART I. SOLIDS MIXING

J. D. Gabor
A.I.Ch.E. Journal 11, 127-129 (Jan 1965)

LATERAL TRANSPORT IN A FLUIDIZED-PACKED BED. PART II. HEAT TRANSFER

J. D. Gabor, B. E. Strangeland, and W. J. Mecham
A.I.Ch.E. Journal 11, 130-132 (Jan 1965)

EFFECT OF METALLIC ADDITIVES ON MERCURY CORROSION OF TITANIUM

J. Y. N. Wang
Corrosion 21(2), 57-61 (Feb 1965)

FINS IN SERIES

T. R. Bump
A.I.Ch.E. Journal 11, 174 (Jan 1965) Letter

SOME IDEAS ABOUT THE MECHANISM CAUSING TWO-PHASE CRITICAL FLOW

H. K. Fauske
Appl. Sci. Res. A13, 149-160 (1964)

STATISTICAL ERROR-ESTIMATION FOR THE TRANSFER-FUNCTION MEASUREMENTS OF A NOISY REACTOR SYSTEM

Chun Hsu and W. C. Lipinski
Nucl. Sci. Eng. 21, 407-408 (March 1965) Letter

THE Z-TRANSFORM OF A PRODUCT OF TWO FUNCTIONS

Isaac Kliger and W. C. Lipinski
IEEE Trans. AC-9(4), 582-583 (Oct 1964)

HEAT TRANSFER WITH LAMINAR FLOW IN A CONCENTRIC ANNULUS WITH PRESCRIBED WALL TEMPERATURES

Raymond Viskanta
Appl. Sci. Res. A12(6), 463-476 (1964)

THE PREDICTION OF LIQUID SUPERHEATS REQUIRED FOR INITIATION OF NUCLEATE BOILING IN THE LIQUID METALS

R. E. Holtz

ASME Technical Digest of the Mechanical Engineering Journal 87(2), 77 (Feb 1965). Presented at the ASME Annual Winter Meeting, Nov. 29 through Dec. 4, 1964, New York. ASME Paper No. 64-WA/HT-31

ANL Reports

ANL-6771 CALORIMETRIC METHODS FOR THE ASSAY OF FUEL PINS AND RESIDUES
N. M. Lazar, S. Rosen, and A. B. Shuck

ANL-6861 THE CONTROL OF CONDENSATION HEAT TRANSFER RATES USING AN ELECTROMAGNETIC FIELD
Ralph M. Singer

ANL-6864 EBR-II WET CRITICAL EXPERIMENTS
F. S. Kirn and W. B. Loewenstein

ANL-6902 ENGINEERING DEVELOPMENT OF FLUID-BED FLUORIDE VOLATILITY PROCESSES. Part 6. Preparation of Dense Uranium Dioxide Particles from Uranium Hexaflouride in a Fluidized Bed
Irving E. Knudsen, Norman M. Levitz, and Albert A. Jonke

ANL-6917 ON THE POSSIBILITIES FOR THERMAL NEUTRON IMAGE INTENSIFICATION
Harold Berger

ANL-6924 THE NONDESTRUCTIVE TESTING OF BRAZED JOINTS
Akira Kannō

ANL-6939 SELECTION OF THE STRUCTURAL MATERIAL FOR THE FARET LIQUID-METAL SYSTEMS
L. R. Kelman and R. J. Dunworth

ANL-6941 A RE-EVALUATION OF FISSION RATIOS MEASURED IN ZPR-III CRITICAL ASSEMBLIES
William G. Davey and Paul I. Amundson

ANL-6951 EVALUATION OF PHYSICAL PROPERTIES OF GASES AND MULTICOMPONENT GAS MIXTURES
John T. Holmes and Manfred G. Baerns

ANL-6958 DEVELOPMENT OF A FLUOROSCOPE FOR STUDYING TWO-PHASE FLOW PATTERNS
John Johanns

ANL-6972 CONSISTENT HEAVY-ATOM CROSS-SECTION EVALUATION FOR PLUTONIUM RECYCLE CALCULATIONS
D. P. Moon

ANL-6980 A STUDY OF THE INITIATION OF NUCLEATE BOILING IN THE LIQUID METALS
Robert E. Holtz